DIPLOMARBEIT / DIPLOMA THESIS

Titel der Diplomarbeit / Title of the Diploma Thesis

Use of dynamic mechanical analysis for the study of glass forming liquids: relaxation dynamics and confinement effects

verfasst von / submitted by

Mag. phil. Dr. Madalina-Roxana PUICA

angestrebter akademischer Grad / in partial fulfilment of the requirements for the degree of

Magistra der Naturwissenschaften (Mag. rer. nat.)

Wien, 2016 / Vienna, 2016

Studienkennzahl lt. Studienblatt / degree programme code as it appears on the student record sheet:	A 190 412 406
Studienrichtung lt. Studienblatt / degree programme as it appears on the student record sheet:	Lehramt UF Physik UF Mathematik
Betreut von / Supervisor:	Ao. Univ.-Prof. Mag. Dr. Wilfried Schranz

ABSTRACT

This thesis describes a number of techniques that have been employed to measure the temperature of the glass transition (T_g) but focuses on dynamic mechanical analysis (DMA), our method of choice to perform elasticity measurements through oscillatory experiments. Our work investigated the low molecular weight glass-forming liquid phenyl salicylate (salol) confined in Vycor 7930 and Gelsil matrices, and was carried out using a Perkin Elmer series 7 DMA instrument.

Our low-frequency measurements of the elastic susceptibility of salol confined to Vycor glass demonstrate that DMA constitutes a very sensitive method to test the dynamic behaviour of glass-forming liquids in confined systems. This technique allows to investigate if there is an "intrinsic" confinement or size effect that is compensated by surface effects. Our results indicate that for decreasing pore radius, the second anomaly in the loss modulus becomes more pronounced, and as such it makes it easier to distinguish confinement and surface effects for pore sizes that approach the correlation length.

Our complex elastic susceptibility data can be fitted well assuming two types of dynamic processes, a "bulk" relaxation in the core of the pores and a radially increasing "surface relaxation" of molecules in the vicinity of the pore surface. The core relaxation time decreases with decreasing pore radius, and the confinement-induced acceleration of dynamics causes a shift in T_g inversely proportional to the pore radius. Our measurements also suggest that the main cause for the T_g shift is a confinement-induced hindering of cooperativity.

The main effect of the confinement is, most likely, to suppress cooperative motion. Consequently, negative pressure effects, while always present, do not have a major contribution to the T_g shift in confinement.

This thesis also reviews subsequent applications and extensions of this work, as well as various models to analyze the experimental data, and alternative experimental techniques.

ZUSAMMENFASSUNG

Die vorliegende Arbeit beschreibt verschiedene Methoden, die bei der Bestimmung der Temperatur des Glasübergangs (T_g) eingesetzt werden, insbesondere die dynamisch-mechanische Analyse (DMA), welche die Elastizität einer Probe durch Oszillationsexperimente ermitteln. Es wurde die glasbildende Flüssigkeit Phenyl-Salicylat (Salol) in porösen Vycor 79330 und Gelsil Matrizen mit einem Perkin Elmer Serie 7 DMA (dynamisch-mechanischem Analysator) untersucht.

Die durchgeführten niederfrequenten Messungen der elastischen Suszeptibilität von Salol in Vycor zeigen die Sensitivität von DMA-Messungen bezüglich des dynamischen Verhaltens von glasbildenden Flüssigkeiten in den Poren einer eingeschränkten Geometrie auf. Diese Methode ermöglicht zu ermitteln, ob "intrinsisches" Confinement beziehungsweise ein Effekt der Porengröße vorliegt, der durch Oberflächeneffekte kompensiert wird. Die Resultate zeigen eine Verstärkung der zweiten Anomalie bei abnehmendem Porenradius. Daraus ergibt sich eine leichtere Unterscheidbarkeit zwischen Confinement und Oberflächeneffekten bei Annäherung des Porenradius an die Korrelationslänge.

Die Daten bezüglich des komplexen elastischen Moduls E* können unter der Annahme des Auftretens zweier unterschiedlicher dynamischer Prozesse ausgezeichnet durch eine entsprechende Ausgleichsfunktion dargestellt werden. Einerseits findet in der Hauptmasse im Porenkern ein Relaxationsprozess statt, andererseits tritt ein weiterer im Bereich der Porenwand auf, welcher mit steigendem Porenradius ausgeprägter wird. Die Relaxationszeit des Porenkerns verringert sich mit Verringerung des Porenradius und die durch das Confinement induzierte Beschleunigung der Dynamik verursacht eine zum Porenradius indirekt proportionale Verschiebung von T_g.

Höchstwahrscheinlich liegt der Haupteffekt des Confinement in der Unterdrückung der kooperativen Bewegung. Daraus folgt, dass die permanent präsenten Effekte des negativen Drucks nicht den überwiegenden Beitrag zum Verschub von T_g leisten.

Außerdem werden auf der vorliegenden Arbeit aufbauende Anwendungen und Erweiterungen, alternative experimentelle Methoden, sowie verschiedene rechnergestützte Modelle zur Auswertung dieser alternativen experimentellen Daten präsentiert.

Content

Chapter 1

1. INTRODUCTION

A major development of elastic measurements over the last 35 years is represented by the use of dynamic mechanical analysis (DMA) techniques to examine elastic instabilities caused by structural phase transitions (*1*). The glass transition, also known as the glass-liquid transition, is a reversible transition that commonly occurs in most amorphous materials (*2*), from a more rigid ("glassy", or hard) state to a softer ("rubbery", or molten) state. The glass transition can also occur in semicrystalline materials, within their amorphous regions.

Determining the temperature of the glass transition (or the so-called "laboratory glass transition temperature" (*3*)), T_g, represents a basic measurement carried out on an amorphous material. Transitions in materials are generally associated with different cooperative motions of molecular segments, whether localized, medium-range, or long-range. Polymer chains are a good example of chain segments whose cooperative motion defines the glass transition (*4*). T_g is the temperature where a material changes state as described above. This change constitutes a sharp transition in the flexibility and viscosity of the material and an increase in its heat capacity. In polymers, it is underlined by a significant increase in the mobility of the polymer chains within the polymer matrix. However, despite these highly substantial changes, the glass transition is not an actual phase transition (*5, 6*).

Based on the aforementioned changes in physical properties that the material undergoes during its glass transition, several techniques have been employed to measure T_g. The most widely used methods are DMA and differential scanning calorimetry (DSC), also known as heat capacity spectroscopy, which monitors the change in the heat capacity of polymers and other macromolecules in the region of the glass transition (*7, 8*). The relation between the specific heat of a solid and its elastic moduli was first formulated by Einstein over a century ago (*1*). DSC was patented in 1962 by E.S. Watson and M.J.

O'Neill (*9*), and two years later the first adiabatic DSC instrument was developed (*10*). DSC has been widely used to measure T_g and for thermal analysis in general (*7, 11, 12*); for example, in polystyrene it was used to follow the change of T_g with the decreasing size of the phase (*13, 14*). Temperature-modulated DSC (TMDSC) was first described in 1993 (*15-17*) and has also since become a well-established technique for thermal analysis, including the study of glass and melting transitions (*7, 11-13*).

Given that the size of the "cooperatively rearranging regions" (as described by G. Adams and J.H. Gibbs, (*18*)) within the material is increasing when approaching T_g, several other experimental techniques have been used to assess the growing length scale for this characteristic correlation length, which is thought to be on the order of nanometers, or some other marker of dynamic heterogeneity (*7, 18-20*). Besides DSC, these techniques include dielectric spectroscopy (*21-23*), atomic force microscopy (*24*), nonresonant spectral hole burning (*25*), static and dynamic light scattering (*20, 26, 27*), multidimensional NMR (*28-32*), and molecular dynamics simulations (*33, 34*).

Dielectric spectroscopy, also known as impedance spectroscopy, is a technique used to measure the dielectric properties (real and imaginary components of the complex dielectric permittivity) of a medium over a frequency range. Broadband dielectric spectroscopy has been used to study the dynamics of the glass-forming liquid phenyl salicylate (salol) (*22*), given that the relaxation process of the dielectric loss (i.e., the imaginary component of the dielectric permittivity) was found to be related to the glass transition (*35, 36*).

Atomic force microscopy is a type of scanning tunneling microscopy or scanning probe microscopy, that can attain a resolution on the order of ångströms (*37*). This technique was used to study dielectric properties in polyvinyl-acetate films at and near the glass transition. The cooperative length scale can be determined from the anomalous variations seen in the low-frequency (1/f) fluctuation (noise) spectrum (*24*).

Spectral hole burning (SHB) represents the bleaching of the absorption spectrum at a selected frequency; the so-called "spectral hole" refers to the increased transmission at the respective frequency. Low-frequency, large-amplitude electric fields were used for dielectric SHB in the nonresonant dielectric relaxation of supercooled liquids, such as propylene carbonate and glycerol. This procedure is applicable not only to viscoelastometry, but also to other techniques, such as magnetometry and photon correlation spectroscopy (*25*).

Light scattering is another method that can be used to investigate glass-forming liquids. Static light scattering experiments reveal long range density fluctuations for 1,1'-di(4-methoxy-5-methylphenyl)cyclohexane (BMMPC) with correlation lengths of up to 185 nm. Intriguingly, such lengths are not consistent with conventional liquid state theories. From the perspective of these theories, dynamic light scattering studies also reveal some unexpected features. Generally speaking, the excess scattering measured indicates a correlation length of 20-200 nm, and light scattering data suggest the existence of a metastable nonequilibrium state for a supercooled viscoelastic liquid also above T_g (*26*). Further dynamic light scattering studies, combined with viscosity experiments and photon correlation spectroscopy, established the temperature-dependent characteristic length for the glass transition in ortho-terphenyl, a parameter that decreases as the temperature increases (*20*).

Solid-state nuclear magnetic resonance (NMR) spectroscopy is a type of NMR spectroscopy in which orientation-dependent (anisotropic) interactions are detected in the spectrum, thus rendering a solid-state NMR spectrum very broad. Supercooled liquids exhibit spatial heterogeneities in the vicinity of T_g (*38, 39*). Solid-state NMR can determine the length scale of such a dynamic heterogeneity (*29*), in a four-dimensional experiment (*32*) that combines obtaining information about reorientation times with measuring the length scale of regions with different dynamic characteristics by spin diffusion (*40*). Multidimensional NMR experiments have been used to measure the length scale of regions of dynamic heterogeneity in o-terphenyl (*29*), supercooled D-sorbitol (*28*), glycerol (*29, 41*) and poly(vinyl acetate) (PVAc) (*29, 32*). Another application for multidimensional NMR exchange experiments is to determine the rate memory for polymers slightly above their T_g (*31*). Moreover, a four-dimensional, as well as a two-dimensional NMR experiment, were used to study slow dynamics in PVAc (*30*).

An alternative and also a valuable addition to the experimental study of glass-forming liquids is represented by computer simulation methods. Molecular dynamics (MD) simulations have shown, for example, that single particle properties are significant for the kinetic transition that happens at a temperature lower than T_g (*33*). A similar approach was used to assess the dynamics of silica (*34*), a strong glass former (*42*). Considering different system sizes shows unexpectedly large finite size effects to be present in simulations of silica dynamics. Furthermore, these effects affect the relaxation times pertaining to the intermediate scattering function, but to a much lesser extent if the system is compressed to high density and thus transformed into a fragile glass former (*34*).

Chapter 2

2. EXPERIMENTAL SETUP

2.1. Dynamic Mechanical Analysis

Dynamic mechanical analysis (DMA) is a technique also known as dynamic mechanical spectroscopy, DMA spectroscopy, dynamic thermomechanical analysis, dynamic mechanical thermal analysis, forced oscillatory measurements, or dynamic rheology (*43*). By a very brief definition, the DMA technique represents the analysis of a material's response to an oscillatory force applied to it (*43*). Thus, a DMA instrument assesses changes in mechanical behaviour as a function of time, temperature, frequency, stress, or combinations thereof. Forces applied in a DMA experiment could be anywhere between the order of newtons to the order of tens of μN (*1*); forces are even smaller when optical tweezers are used or in atomic force microscopy (*44, 45*). One can achieve even forces on the order of fN (*46*), which are needed to study the strain-stress relationship in soft biological systems (*47-49*).

The history of DMA is part of the century-long history of elasticity measurements through oscillatory experiments (*43, 50-52*). Dynamic measurements were described by J.D. Ferry, M.L. Miller, and N.G. McCrum et al. in the 1960's, in their classic books on polymer properties (*2, 53, 54*). During the same decade, DMA entered its modern period, through the development of the torsional braid analyser by J. Gillham (*55*), followed by a couple of other DMA instruments that also used the torsional geometry. The first dynamic mechanical thermal analysers that used an axial geometry became available in the early 1980's, followed by the higher-sensitivity controlled stress analyser built by Perkin Elmer, using their new thermomechanical technology (*43*).

DMA is one of the three approaches that have been developed to allow the possibility of analyzing the elastic response of moving interfaces. A second technology is related to torsion pendulum arrangements (*56-59*), but it presents major disadvantages, due to the large sample size and to the difficulties of inserting the sample into the instrument (*1*). The other category of techniques includes the local ones, relevant for the minute geometrical size of the exciting elastic force. Atomic force microscopy, nanoindentation methods, and optical tweezers all employ an elastic force that is concentrated to the scale of interatomic distances, and as such making them ideal tools for assessing local response fields, especially in biological systems (*1, 60-62*).

The use of DMA techniques to analyze elastic instabilities caused by structural phase transitions represents a major development of elastic measurements over the last 35 years (*1*). DMA has been shown to be the most sensitive thermal technique available for the purpose of determining T_g, given the sharp change in flexibility that occurs at this temperature. Compared to DSC, not only is DMA considered to be more sensitive by about an order of magnitude, but it can also be used to obtain a parameter not available in DSC measurements, namely the coefficient of thermal expansion, which is a measure of a material's expansivity (*43*).

DMA applications to the study of material properties extend well beyond glass transitions, i.e. beyond determining T_g. Generally speaking, one can investigate not only the temperature response, but also the frequency response of a material to stress; moreover, even the problem of the temperature response is more complex than discussed so far. For example, plotting the elastic modulus against temperature in nylon can reveal changes in E' at lower temperatures. Thus, the glass transition is designated as α transition ($T_g = T_\alpha$), which is associated with the gradual chain movement, and the subsequent transition, designated as β transition, represents pendant group or side chain movements, indicative of the toughness of the polymer (*43, 63-67*). In an ideal representation, shown in Figure 1 (*43*), each transition revealed by the DMA analysis represents a molecular relaxation associated with a certain type of molecular motion.

This information could also allow for the determination of the operating range of a given polymer. Unlike DSC, DMA has the sensitivity to detect the β and γ transitions (*68*), and also to determine T_g in thin coatings or in highly cross-linked thermosets (*43*).

Another application of DMA employed to study polymers pertains to their composition. The results of the DMA analysis are altered by the composition of monomers and also by cross-linking, that can change or add the functionality of the polymer. The miscibility is another property of polymers that can be effectively evaluated using DMA. Plotting the storage modulus for a variety of blend ratios will reveal various profiles, from a steep drop-off to a broader transition featuring a shoulder. Such differences reveal a lack of homogeneity in the respective areas. Besides the effect of blend ratios, the DMA analysis can also determine the role of curing agents and that of fillers (*69*).

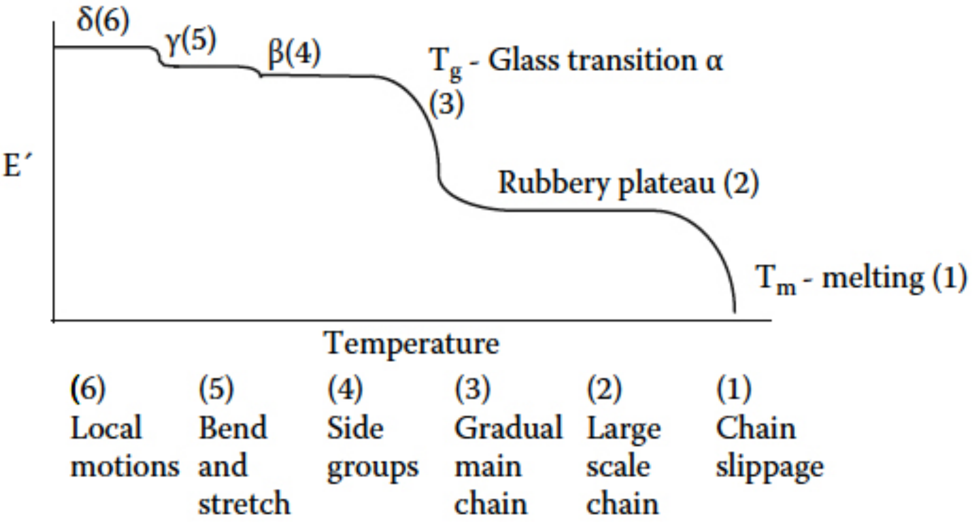

Figure 1. The effect of the different types of molecular relaxations on the idealized representation of a temperature scan of the storage modulus (reproduced from (43)).

For the DMA study of thermosets, tracking modulus or viscosity changes allows one to follow the material all through its curing. One can thus determine the initial melting of the material before curing (that corresponds to the minimum value of the viscosity and of the modulus), and then the increase in viscosity during curing towards the solid state (*43*). For an epoxy resin, DMA allows one to estimate the point where the material is gelled (the point of gellation), how fluid it gets (the minimum viscosity), and the point where it is stiff enough to be able to bear its weight (*43, 70*). By following the increase in viscosity during curing, one can also estimate the activation energy (*71*). This energy can be determined more accurately by using isothermal runs (*72*).

As mentioned above, the frequency response of a material to stress encompasses another range of DMA applications. This method is applied to the study of the viscosity and elasticity in a wide range of materials, including polymer melts, solutions, and suspensions (*43, 73-76*). In a hot melt adhesive, the low-frequency response of the modulus describes stickiness or tack, whereas its high-frequency response describes the peel resistance (*73*).

Creep-recovery testing is a particular case of DMA experiment and yet a fundamental analysis of material behaviour and a powerful analytical tool (*43, 77*). This test involves applying a constant load, determining the response of the material to it, and subsequently removing the load and again examining the material's behaviour. This sequence of events can be repeated over multiple cycles. The properties determined during a creep-recovery experiment are modulus and viscosity, and they allow one to predict the material's behaviour under real-life conditions (*43*). Data can be collected at very low frequencies during the creep experiment (*78*), and at high frequencies during the recovery (*79*).

Consequently, the versatility and wide applicability of dynamic mechanical analysis makes it useful for the study of either the temperature behaviour or the frequency behaviour of numerous materials, ranging from suspensions, solutions, and colloids to polymer melts, and to solid composites (*43, 69, 80*).

2.2. Instrumentation

The experiments described in this study have been performed using a Perkin Elmer series 7 dynamic mechanical analyser. This instrument was first built in 1989 and has since been commercially available from Perkin Elmer, Inc. (Waltham, MA, USA). A picture of this instrument is shown in Figure 2 below.

Figure 2. The Perkin Elmer series 7 dynamic mechanical analyser (reproduced from (*81*)).

In a DMA apparatus, the sample is exposed to a static force modulated sinusoidally by a dynamic force of a certain amplitude and frequency. The dynamic elastic modulus, E, is determined from the amplitude and phase shift of the elastic response (*1*). Thus, DMA is used to measure various properties of materials while being deformed under a sinusoidal stress: storage and loss modulus (i.e., viscoelastic moduli: the real, E’, and imaginary, E”, components of the complex E), damping (energy dissipation as heat) properties, and tangent delta or Tan delta (the loss factor, defined as the ratio of loss to storage modulus). Modulus reflects the elastic response of the material (the oscillating sample response in phase with the oscillatory force), whereas damping describes the viscous response.

Using DMA equipment that is currently commercially available, such as the Perkin Elmer DMA7 and Diamond DMA instruments, the above listed parameters can be measured over a frequency range of 0.01-50 Hz (100 Hz for Diamond DMA) and a temperature range of 90-850 K (120-850 K for Diamond DMA) (*1*); the latter can be extended down to 15 K for DMA7 by adding a cryostat (*82*). Both Perkin Elmer instruments allow for the application of a minimal force of 1 mN, whereas the maximal force is 2.5 N for DMA7 and 10 N for Diamond DMA (*1*). The resolution of the force is 10 μN for both instruments.

The Perkin Elmer DMA7 analyser can be operated in several different modes, the most often used being time scan (isothermal) and temperature modes. T_g can be defined using any of the following three parameters that are continuously assessed during a DMA experiment (Figure 3 (*83*)):

- from the storage modulus: E’ onset (sharp decrease) arises at the lowest temperature and is associated with mechanical failure (*4*);

- from the loss modulus: E” peak is reached at the middle temperature and reflects molecular processes. As such, it describes T_g as the temperature at the inception of segmental motion and thus it relates to the changes in physical properties commonly associated with the glass transitions in plastics;

- from the tangent delta: In this approach, historically used in the literature, the Tan delta peak corresponds to the highest temperature. For a polymer, it represents the midpoint between the rubbery (softer) and the glassy (more rigid) states, and the amorphous content of the polymer determines the shape and height of the peak (*4*).

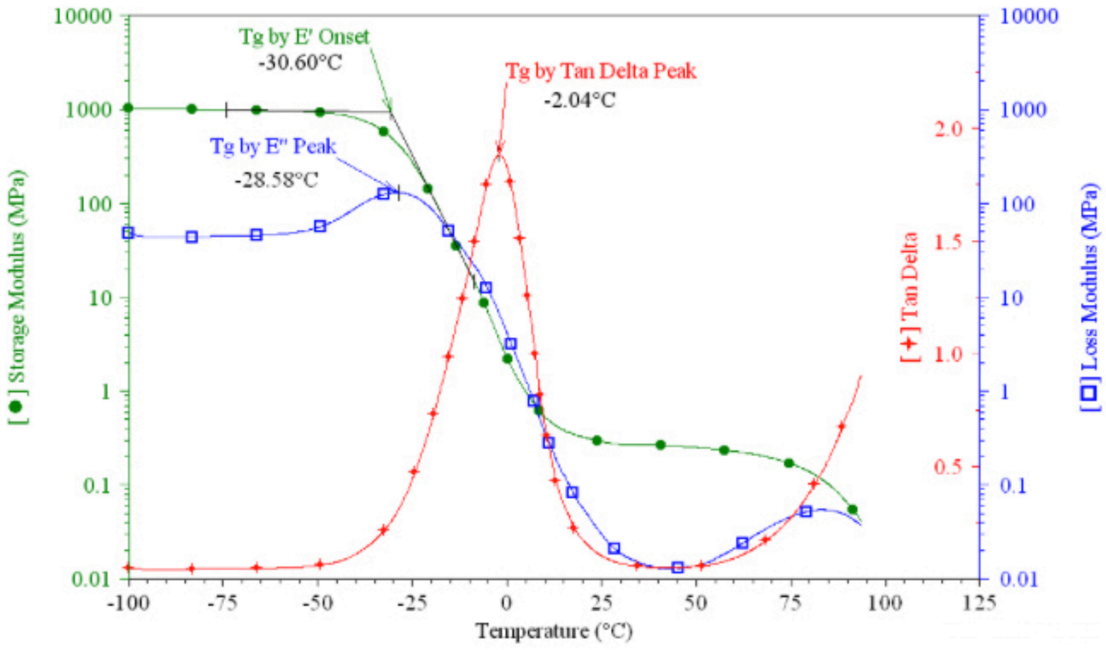

Figure 3: Three different methods have been used to determine the temperature of the glass transition in a dynamic mechanical analysis experiment. Shown in this example is a scan of a self-stick, or pressure-sensitive adhesive (PSA) run in tension clamps with the following parameters: frequency = 1 Hz, amplitude = 10 μm, and ramp rate = 5 °C /min (reproduced from (*83*)).

The differences among these three temperature values are observed experimentally (Figure 3), thus demonstrating that in actuality the glass transition occurs, usually, over a temperature range instead of a single temperature.

The DMA7 instrument consists of several main components: a measuring system assembly and a central core rod, a linear variable differential transformer (LVDT) sensor to detect displacement (the change in the position of the rod that occurs in response to the applied force) with high sensitivity, a fast-response furnace and a linear force motor. In principle, in order to perform DMA measurements, the sample is confined between two restraining elements or grips, and a dynamic (sinusoidally modulated) force is applied to it using an electric motor. The resulting displacement is measured using a force transducer or a LVDT sensor. The storage modulus, the loss modulus, and/or the Tan delta are then plotted against temperature, as shown in Figure 3

Figure 3. The Perkin Elmer DMA7 and Diamond DMA instruments are most often used in two geometrical arrangements, the parallel plate stress and the three point bending, shown further below in Figure 14 (*1, 81, 84*).

In the parallel plate (PP) stress geometry, the force is applied in a certain direction and the resulting change in length is measured in the same direction. Both Perkin Elmer DMA instruments can resolve changes in length of about 10 nm, but a three point bending (3PB) experiment allows for a higher resolution. A 3PB experiment also allows for a more efficient optimization of the sample geometry than a PP experiment (*1*). Moreover, in the 3PB configuration the length L is generally fixed (as defined by the sample holders), and varying the sample thickness h modulates the effective spring constant. In this configuration, the static component of the force ensures that the sample stays in contact with the sample holders (knife edges) at all times. The dynamic component of the force has a frequency in the range of 0.01-50 Hz. The amplitude of the peak deformation and the phase lag of the response (the phase angle between the stress sinusoid and the strain sinusoid) are measured through electromagnetic inductive coupling; the measurement resolution is on the order of 10 nm in amplitude and 0.1° in phase (*1*). The spring constant, damping, and Tan delta are calculated from the amplitude and phase lag of the response; the storage (elastic) modulus and the loss (imaginary) modulus are then calculated from these parameters.

Temperature control is achieved with heating and cooling accessories. A heater surrounds the sample chamber and is itself surrounded by a continuously flushed water bath. A furnace filled with liquid nitrogen ensures the cooling of the sample. Temperature control can be achieved within 0.1 K and it has been verified by performing heating and cooling runs between 180 and 900 K (*81*).

Calibration of force, height, and deformation is performed using standard calibration samples per the manufacturer's recommendations. All these calibrations need to be repeated whenever the geometrical arrangement is changed. Calibration of the thermocouple is performed using indium standards provided by the manufacturer, by determining the change in the rod position upon the melting of the indium piece, whose melting point is 429.75 K. Subsequent measurements are corrected by the difference between the measured melting temperature and the above mentioned literature value (*81*).

2.3. Porous Glasses

2.3.1 Vycor 7930

The Vycor® brand glass is a commercial glass manufactured by Corning, Incorporated (Corning, NY, USA), which has been available for more than half a century. Porous Vycor® glass and other porous materials are used in a wide range of applications and products, including: sensors, detectors, high performance liquid chromatography (HPLC) frits, gas, liquid and petroleum separation, gas adsorption, filters, vacuum chucks, reference electrodes, various medical devices, lasers and optics.

Vycor code 7930 is almost pure vitreous silica (silicon dioxide), with a composition of 96.3% silica (SiO_2), 2.95% boron trioxide (B_2O_3), and 0.04% sodium oxide (Na_2O) (% w/w). Most of the remaining content is composed of Al_2O_3 + ZrO_2 (*85*). It is a chemically inert, mechanically hard and strong, non-flaking, non-dusting material.

Preparation of porous silica glasses originated in the discovery made in 1926 by Turner and Winks (*86*) and in the patent developed subsequently by Nordberg and Hood (*87*). This special process circumvents the requirement for high temperatures in forming and melting, by replacing it with the following sequence: conventional melting, standard shaping at a larger size, heat treatment below the deformation temperature but above the annealing point (the so-called "demixing" step, that yields two glassy phases), soluble phase removal by leaching (through immersion of the glass in a hot solution of dilute acid), which produces the porous glass, and consolidation of the porous structure by slow heating to temperatures above 1200 °C (*88*). The acid leaching process takes advantage of the fact that the silica-rich phase of the mixture is insoluble in acids, whereas the other phase, rich in B_2O_3 and alkali, is readily soluble. For Vycor 7930, the preparation starts with a melt containing 75% SiO_2, 20% B_2O_3, and 5% Na_2O, and after the slow acid leaching of the soluble phase, a solid, but porous skeleton of 96.3% SiO_2 is left behind (*88, 89*). The interconnected microporous structure is evident in electron micrographs, as well as with other techniques, including direct energy transfer, molecular adsorption, and small-angle scattering (*89*).

The temperature of the demixing step, described above, determines the pore size obtained in the Vycor glass, i.e. the pore diameter can be modified by altering this parameter. Demixing temperatures below 500 °C generate smaller pores, with diameters as low as 50 nm, whereas higher temperatures (on the order of 700 °C) generate larger pores, with diameters of 100 nm and more (*90*). These pore sizes were determined either by scanning electron microscopy (SEM) or by using the Brunauer, Emmett and Teller (BET) theory (*91*). Generally, pores with sizes below 2 nm are termed "micropores", whereas "mesopores" and "macropores" refer to pores of 2-50 nm in size and larger than 50 nm, respectively (*92, 93*). The following image (Figure 4) shows a transmission electron microscopy (TEM) micrograph from a Vycor glass section, revealing an isotropic and homogeneous distribution of mass and void (mass corresponding to dark regions and void to white regions).

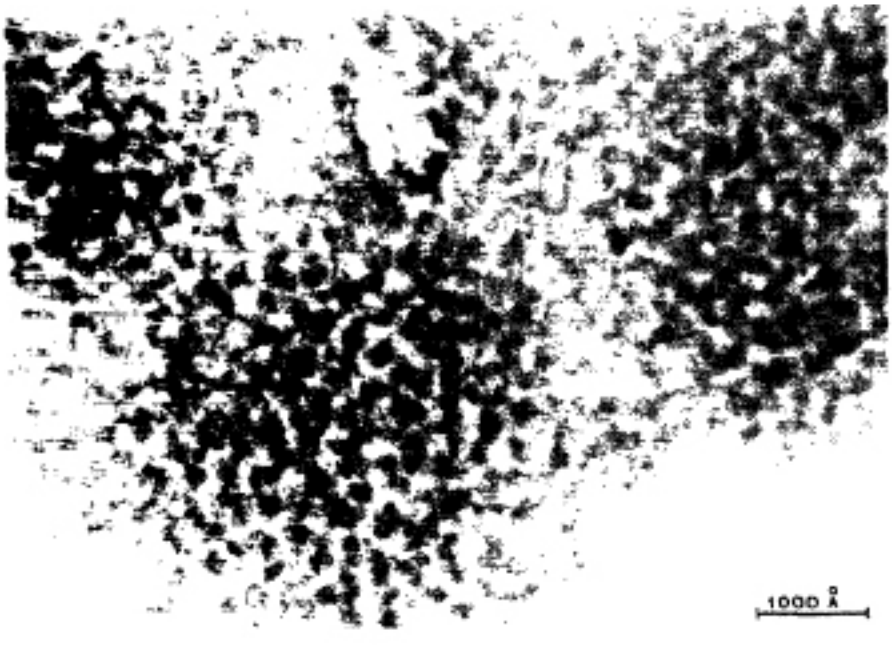

Figure 4: TEM of a ultrathin (30-40 nm thick) section of Vycor 7930 glass (reproduced from (*89*)).

The same Vycor glass lot shown in Figure 5 was characterized by determining its nitrogen adsorption and desorption properties at -196 °C (*89*), and the nitrogen desorption isotherm was analyzed with the BET model (*91*). Accordingly, the desorption data yield a pore size distribution whose peak corresponds to a pore radius of 3.5 nm (*89*).

Ten years later, a similar nitrogen adsorption study was performed on Vycor glass model 7930 using modern instrumentation. Pore radii determined from the adsorption and desorption branches were 5.8 and 3.4 nm, respectively (*94*). These results were compared within the same study with data obtained using optical characterization by spectroscopic ellipsometry, as well as TEM to estimate pore size. The pore radius determined by ellipsometry ranges from 1.5 to 2.1 nm. The difference is most likely due to impurities being placed into the pore walls and to water adsorption reducing the effective radius, given that the ellipsometric measurements were performed under room conditions (*94*). From TEM micrographs (see Figure 5) the authors estimated the pore radius to be 5 nm.

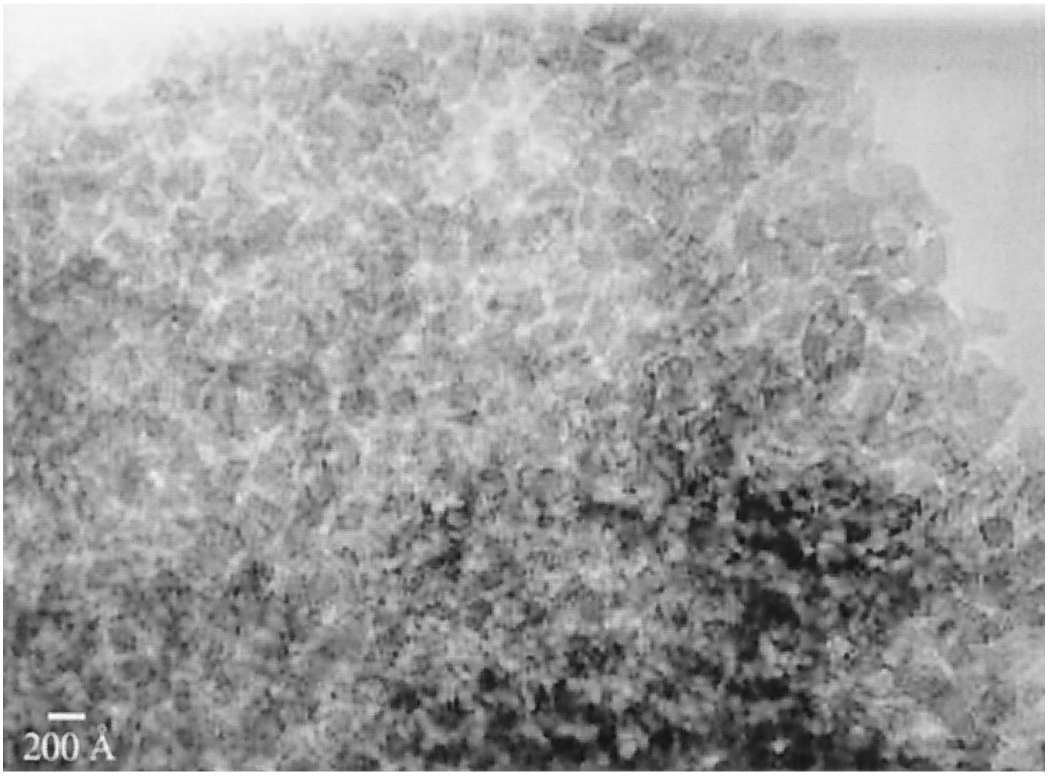

Figure 5: The microstructural appearance of Vycor 7930 glass determined by TEM (reproduced from (*94*)).

More recently, adsorption was used in combination with small-angle scattering (SAS) to study the porosity of Vycor glass (including the effect of pore connectivity and surface curvature on the adsorption process); permeability techniques were also employed for this purpose (*95*).

In our study we used the schematic pore model of Vycor 7930 with interconnected pores and pockets, as shown in Figure 6:

Figure 6: Pore structure of the Vycor glass (reproduced from (*19*)).

The density of Vycor glass was calculated based on weight and volume measurements of commercial samples and was found to be ρ = 1.4 g/cm^3. The total porosity (Φ) of a porous medium is defined as the fractional volume of pores relative to the bulk volume of the material. As such, this parameter can range between 0 and 1, and we have calculated it from the following equation:

$$\Phi = 1 - \frac{\rho}{\rho_b} \qquad [\mathbf{1}]$$

where ρ is the sample density and ρ_b is the density of silica bulk. Using ρ_b = 2.2 g/cm^3 (*88, 89*) porosity is then calculated as 0.36. This result is consistent with previously reported values of 0.40 for untreated Vycor and 0.33 for silanated Vycor (*81, 96*), 0.30 determined through nitrogen desorption or 0.31 through TEM image analysis (*89*), as well as the result of 0.30 that we reported for untreated Vycor (*84*).

2.3.2. Gelsil

Gelsil is the other type of porous silica glass used in our experiments, besides Vycor (*84*). Up until recently, the main manufacturer of Gelsil products was Geltech, Incorporated (Orlando, FL, USA). This series of products has been described extensively (*97, 98*); they are rigid, transparent, highly pure silica xerogels with complex interconnected pores. Gelsil products are used in various applications and products, including as substrates for photovoltaic dyes, optical sensors, catalyst supports, and separation devices (*99*).

As described above for Vycor, Gelsil sample preparation is also a multi-step process, which involves hydrolysis of tetramethyl-orthosilicate (reaction to which a chemical additive is supplemented for drying control), casting, gelation, and aging. Final preparation steps are: drying, dehydration, and densification, with the last step occurring at approximately 900 °C (*99, 100*). Characteristic parameters for Gelsil 200 were determined to be: $\rho = 2.18$ g/cm^3 (determined with the picnometric method (*101*)), $\rho_b = 0.61$ g/cm^3, and thus $\Phi = 0.72$ (*99*). Such a high porosity (twice as much as that of Vycor) describes a highly interconnected pore system within a thin silica skeleton. This is obvious in both three-dimensional (3D) reconstructions and TEM images (Figure 7). Visualizing the thin slices of the 3D reconstructions is necessary because TEM images represent a 3D slice whose thickness far exceeds the size (25 nm) of the agglomerated spheroidal particles that compose the material, and hence few 22 nm pores are visible in Figure 7d (*99*).

Other Gelsil products have been described in the literature, with various characteristics, such as nanoporous Gelsil 2.5, 5.0 and 7.5, in which the pore diameter averages 2.4, 4.6, and 6.8 nm respectively, and the porosity is 0.39, 0.68, and 0.72, respectively (*102*). Gelsil 50 has a pore diameter of 4.5 – 4.6 nm and a porosity of 0.63 (*103*). Experiments have been carried out on Gelsil glasses with pore sizes as high as 20 nm (*104*).

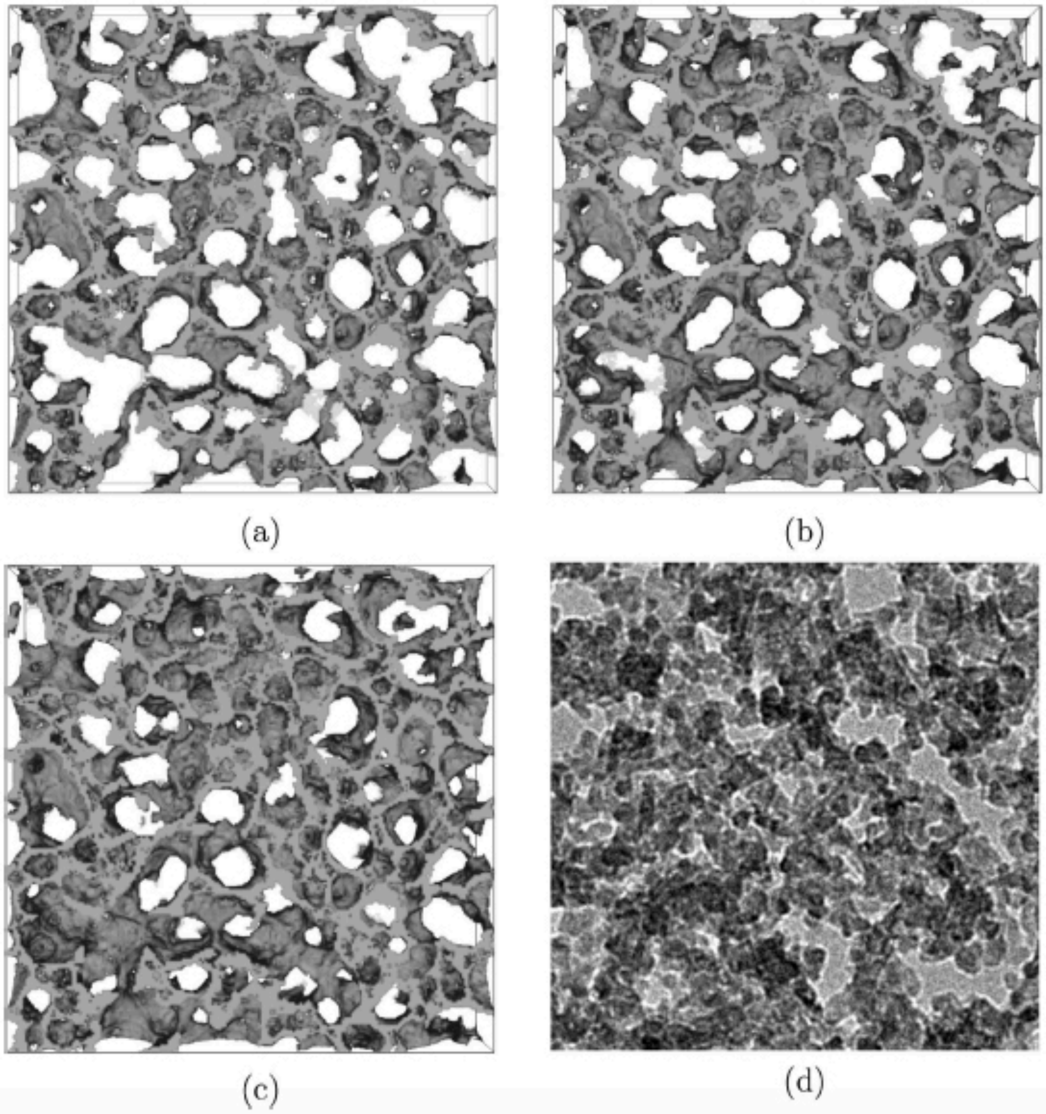

Figure 7: Gelsil 200 imaged by 3-D reconstructions (a-c) and by TEM performed at an operating voltage of 120 kV (d) (reproduced from (*99*)).

2.4. Salol

Phenyl salicylate ("salol", or, according to the nomenclature of the International Union of Pure and Applied Chemistry, phenyl 2-hydroxybenzoate) is a chemical compound ($C_{13}H_{10}O_3$, molecular weight 214.22 g/mol) (*105*), produced by heating of salicylic acid with phenol. Its structure is shown in Figure 8 below. It is used as a preservative, in the prevention of sunburns (as a light absorber in sunscreens), and also in the manufacturing of certain polymers, lacquers, adhesives, waxes, and polishes. This compound also has medical use, as an antipyretic, analgesic, and intestinal antiseptic. Its relevance to our work is due to the fact that it is also a low molecular weight glass-forming liquid.

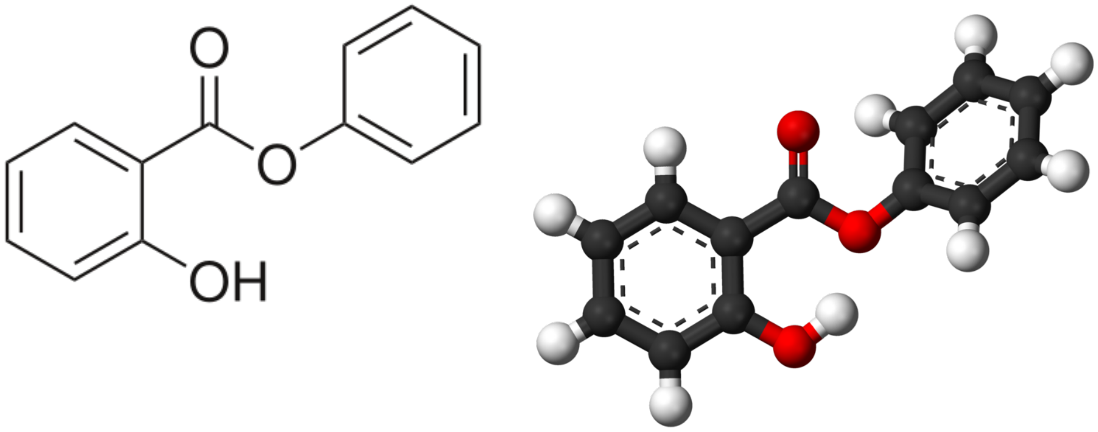

a) b)

Figure 8: Structure of salol: (a) 2-dimensional chemical structure and (b) ball-and-stick model of the salol molecule (available from the public domain).

The melting point of crystalline salol is 42 °C, whereas the T_g of amorphous salol is 50 °C (*105*). Cooling curves for salol in air and in water are plotted in Figure 9.

The molecular dynamics, glass transitions, and other thermal properties of salol in confinement have been studied in porous uniaxial anodic alumina oxide membranes of various pore sizes (13-100 nm in diameter) using dielectric spectroscopy and DSC (*105*).

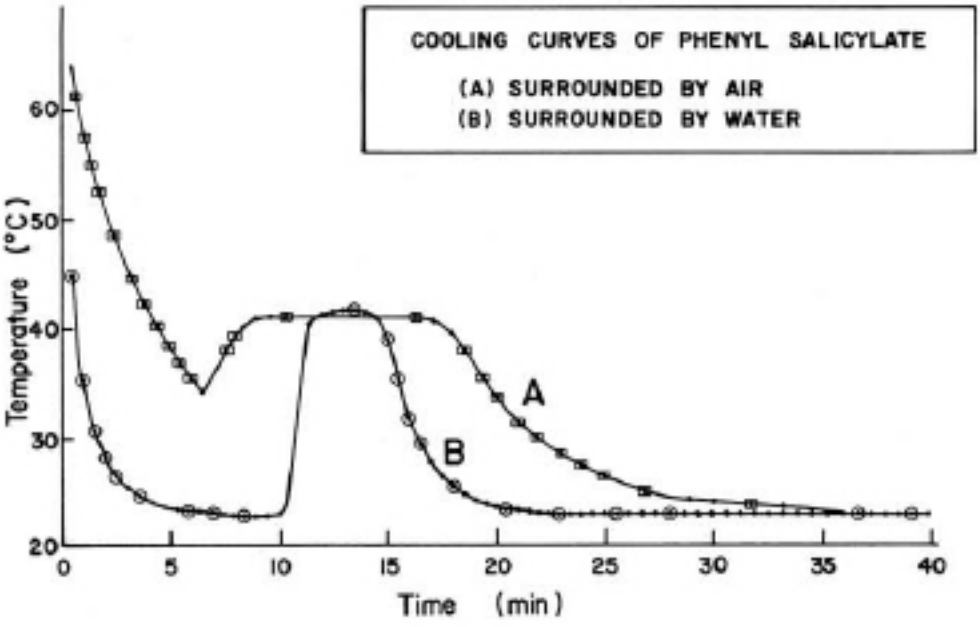

Figure 9: Phenyl salicylate (salol) cooling curves in air and in water (reproduced from (*106*)).

The "fragility" of a glass former measures the deviation of the relaxation behaviour of the respective material from the Arrhenius activated kinetics (*107*), or the "abruptness" with which its dynamics slows down as it approaches T_g (*108, 109*). The origin of this fragility remains one of the most intriguing questions related to the glass transition (*107*). The fragility of a glass former was shown to be directly proportional to the ratio of the bulk and shear moduli of the material (*110, 111*). This parameter is thought to be a measure of the cooperativity of dynamics for a glass former, i.e. a more fragile glass-forming liquid possesses a higher degree of dynamic cooperativity (*18, 109*). For salol, the fragility index was found to be 73 (*112, 113*). Intriguingly, on the one hand the fragility modulates the strength of the confinement effects on T_g (*114*), but on the other hand it can also be affected by nanoconfinement (*115-121*).

2.5. Sample Preparation

In order to use DMA to calculate Young's modulus in bending or compressing mode, we used geometrical models that require rectangular sample shapes. Consequently, the silica glass samples have to be processed so that they have parallel sides and orthogonal corners. This involves cutting and sanding: the manufactured rods were cut into discs using a diamond wire saw, and then cut again into bars; finely grained sandpaper was subsequently used to sand the bars mounted on special U-shape steel support, until they achieved orthogonal corners and parallel sides. The shape and angles of these rectangular bars were regularly checked during the process with an optical microscope. The sequence of mounting, sanding, checking, and rotating the samples was repeated until the desired result was achieved with an accuracy of 10 µm or less.

After preparation, porous glass samples have to be cleaned in order to remove organic impurities that can be absorbed from the atmosphere alongside water, and that produce a color change in the glass, which thus turns brown or yellow with time. Removal of absorbed organic contaminants was performed by boiling the samples in 30% H_2O_2 solution for 24 hours (*88*). An alternative cleaning method, not used in the present study, involves immersing the samples in nitric acid (or another oxidizing acid) containing a small amount of potassium or sodium chlorate. Besides wet oxidation methods, one can also remove absorbed organic impurities by gradual heating of the glass in oxygen or air to 500 °C and maintaining the samples at this temperature until the oxidation removes all contamination (*88*).

Cleaned samples were subsequently dried in a vacuum chamber (10^{-6} mbar) for 24 hours at 120 °C and stored short-term in a desiccator, in the presence of dessicant silica bags, or long-term in distilled water. Subsequent transport of cleaned samples was also done in the presence of silica bags, in a desiccator.

Filling of porous glasses with salol was carried out by utilizing capillary forces, which are strong enough to fill the pore space almost completely. However, submersing the glass in liquid salol and ensuring that the entire sample surface is in contact with salol only achieves a partial filling, as pores in the center of the sample remain unfilled, forming a bubble that can no longer be filled. For better results, the sample should be allowed to soak up single droplets of salol, ensuring that only one side remains in contact with the liquid. This approach is the most appropriate one for samples that will undergo DMA analysis, because this filling procedure ensures that none of the sides that touch the measurement setup has previously come in contact with salol. This way, all the measured effects have to be attributed exclusively to the salol located within the pore system (*81*).

Chapter 3

3. HETEROGENEOUS RELAXATION DYNAMICS OF NANOCONFINED SALOL

This chapter includes the manuscript of the published article "Heterogeneous relaxation dynamics of nanoconfined salol probed by DMA", ***Europhysics Letters*** **79, 36003 (2007) by W. Schranz, M.R. Puica, J. Koppensteiner, H. Kabelka and A.V. Kityk (*****19*****).**

“Heterogeneous relaxation dynamics of nanoconfined salol probed by DMA”, Europhysics Letters 79, 36003 (2007)

W. Schranz[1], M. R. Puica[1], J. Koppensteiner[1], H. Kabelka[1] and A. V. Kityk[2]

[1]Nonlinear Physics Group, Faculty of Physics of the University of Vienna -
Boltzmanngasse 5, A-1090 Wien, Austria

[2]Institute for Computer Science, Technical University of Czestochowa - Armii
Krajowej 17, PL 42-200 Czestochowa, Poland

ABSTRACT

We present novel low-frequency (0.1 Hz – 50 Hz) measurements of the complex elastic susceptibility of the glass-forming liquid salol confined to nanoporous Vycor glass. Our data can be perfectly interpreted with the assumption of a radial distribution of Vogel-Fulcher temperatures $T_0(r)$ inside the pores, resulting from an increase of the molecular relaxation time with decreasing distance from the rough pore surface as recently found by computer simulations (Scheidler *et al.*, *Europhys. Lett.* 59, 701 (2002)). The results show for the first time, that the dynamic elastic response is extremely sensitive for separating confinement-induced acceleration effects of the molecular dynamics and surface-induced slowing-down due to rough pore interfaces.

PACS 61.20.Lc – Time dependent properties; relaxation

PACS 62.25.+g – Mechanical properties of nanoscale materials

3.1. Introduction

Dynamics in confined systems is a widely distributed phenomenon. It appears in chemistry, physics, biology and material science. Basic questions concerning the modification of structural phase transitions (*122, 123*), crystallization (*124*), melting (*125-127*) or glass transitions (*128*) under confinement are a matter of active research. Near the glass transition temperature T_g a dramatic increase of the characteristic relaxation time τ or the viscosity over more than 14 decades is observed (α-relaxation) (*129, 130*). This can be interpreted as resulting from a cooperative behaviour of the relevant molecular motions ("cooperatively rearranging regions") characterized by a lengthscale ξ, which increases when approaching T_g (*18, 131*). Close to T_g this correlation length ξ_g is expected to be of the order of a few nanometers (*39, 132*). To search for such a characteristic length scale underlying the glass transition many experiments and computer simulations of glass-forming systems in spatial confinement of pores or ultrathin films have been performed over recent years (*133*). This research is motivated by the following simple idea: If a growing correlation length ξ with decreasing temperature would be at the origin of a glass transition, then a spatial limitation d should lead to a decrease of T_g (confinement-induced acceleration of dynamics due to suppression of cooperatively interacting modes), and finally suppress the glass formation at all for $d < \xi_g$. Indeed dielectric spectroscopy and temperature modulated DSC measurements of polypropyleneglycol (PPG) and polydimethylsiloxane (PDMS) confined to nanoporous silica based host systems yield strong evidence for an inherent length scale relevant for glassy dynamics. *I.e.* the specific heat anomaly at T_g decreases with decreasing pore size and finally vanishes at d = 1.8 nm for PPG and d = 5 nm for PDMS (*134*). There are, however, also systems, where the heat capacity does not disappear even at very small pore diameters, as found, e.g., for o-terphenyl (*135*) and glycerol (*136*). From dynamic calorimetry across the glass transitions of polyethylene-terephtalate, benzoin-isobutyl-ether and salol $\xi(T_g) \approx 2$ nm was found (*137*). For comparison, dielectric measurements of salol confined in nanoporous Gelsil yielded $\xi(T_g) > 7$ nm (*22*). The origin of such discrepancies is a matter of current discussions in terms of calculating the correlation length either using the Gibbs or the von Laue approach (*137*).

A complication of the simple above idea is due to the assumption that surface effects in the pores may balance or even overcome an intrinsic or confinement effect. Samples with uncoated (natural) pores, where H-bonds between the molecules and the walls can form, correspond to the situation of a rough surface. Then the effect of this wall would be to block the molecular motion at the pore surface, slowing down the confinement-induced acceleration of dynamics. This seems to happen in toluene-d3, where it was argued that the surface-induced slowing-down of the molecular motions is transmitted quite far into the pore volume (*138*). This implies, that the surface-induced slowing-down dominates over the finite-size induced acceleration and T_g is effectively shifted to higher temperatures due to confinement. Also for benzene an increase of T_g with decreasing pore size was reported (*139*). Of course for such systems a discussion on the problem of length scales must distinguish between liquids with strong or weak wall interactions making H-bonds with the pore surface or not, etc. (*140*).

If on the other hand the pore surface is coated, the molecules located near the walls would be highly mobile, and one expects an additional acceleration. Such surface effects were recently modeled by molecular-dynamics simulations of the relaxation dynamics of confined glass-forming liquids (*141-144*). Considering two types of confining walls, the authors found a slowing-down or an acceleration of the dynamics close to rough or smooth pore surfaces, respectively. Experimentally, dynamics in confinement is probed by a large variety of techniques like differential scanning calorimetry (*135*), dynamic calorimetry (*137, 145*), dynamic mechanical measurements (*146*), dielectric spectroscopy (*147*), neutron scattering (*148*) or NMR (*149*). Despite the huge number of experimental and theoretical work which report increasing (*136*), decreasing (*135*), constant or even two glass transition temperatures (*150*) for various pore sizes, no final picture of the behaviour of glasses in confined media has been obtained up to now. This is partly due to the diversity of features which real systems show depending on the type and strength of interactions between the molecules and the pore surface, the measuring technique, etc. Excellent discussions concerning these questions can be found in (*140*) and (*151*).

3.2. Experimental Results

In order to investigate the predicted confinement effects on dynamic elasticity, we performed detailed Dynamic Mechanical Analysis (DMA) measurements of the low-molecular-weight glass-forming liquid salol (phenyl salicylate, $C_{13}H_{10}O_3$) confined to nanoporous Vycor glass (code 7930). Vycor is composed of nearly pure SiO_2. The confining morphology of Vycor (7930) can be described as a network of three-dimensional (3D) randomly connected pore segments with a mean pore diameter $d \approx 7$ nm (Figure 10), with a distribution width of ≈ 0.5 nm and an average length $l \approx 30$ nm (*89*) having a porosity of about 28%. The pore segments are uniformly distributed in orientation and density. Salol is a fragile (fragility parameter $m = 73$) glass-forming substance (*112, 113*), which is considered as a model system for the study of glass transition and molecular mobility in the supercooled liquid. It has been extensively studied by many experimental techniques, so that a great deal of information is available for comparison with new experimental and theoretical work. The glass transition temperature of salol ($T_g \approx 220$ K for the bulk material) is moderately lowered in confined geometry. Trofymluk *et al.* (*136*) found a nonmonotonic dependence of T_g on pore size for salol confined in ordered mesoporous silica (MS). For pore sizes of 5.6 – 26.4 nm they determined a depression of T_g of 2 – 3 K. The authors also found that liquid salol does not crystallize in pores < 11.8 nm and easily vitrifies on cooling (*136*). This allowed us to perform the experiments studying the glass transition with moderate cooling and heating rates (2 K/min). Unlike to the confined case bulk liquid salol easily crystallizes at about 290 K and it requires cooling rates of about 500 K/min to supercool it to the glassy state (*152*).

The present measurements have been performed using a Dynamic Mechanical Analyser (DMA7-Perkin Elmer). In this method a static or dynamic ($f = 0.01 – 50$ Hz) force (1 – 2500 mN) is applied. The amplitude Δh (inset of Figure 12) and phase lag δ of the mechanical response are measured via electromagnetic inductive coupling with resolutions of better than 10 nm and 0.01°, respectively.

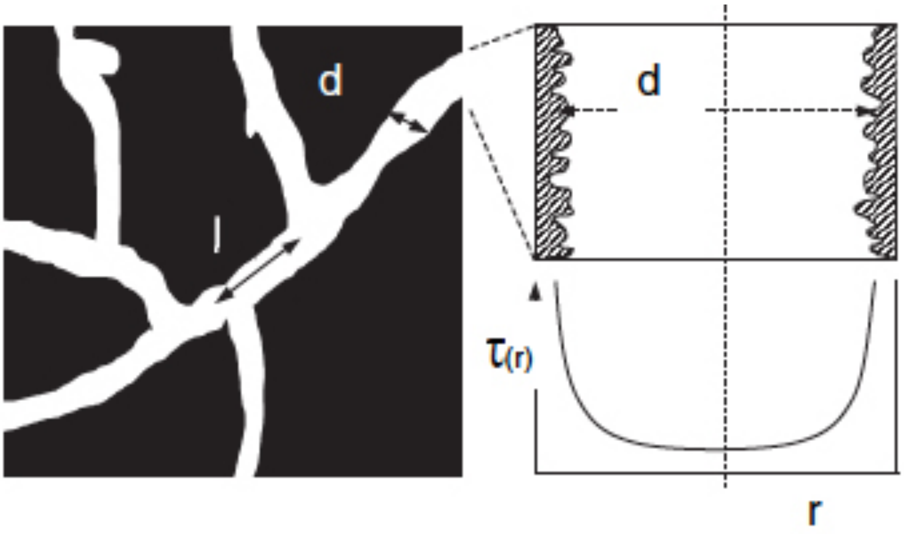

Figure 10: Scheme of the pore structure of Vycor glass. On the right-hand side the increase of the relaxation time of confined salol molecules approaching the rough walls according to simulations of (*142*) is sketched.

This allows to determine the real and imaginary parts of the dynamic elastic susceptibility of a material at low frequencies as a function of temperature and applied force. The measurements are performed in so-called parallel-plate or three-point bending geometries. In contrast to the relative accuracy, the absolute accuracy of the method is rather poor. There are two main sources for systematic errors, i.e. the error due to the DMA Quartz rod-motor system (modeled by a spring constant $k_{DMA} \approx 2 \times 10^4$ N/m) and an error due to non-perfect mechanical contact between the sample and the DMA Quartz rod (we found typical values of $k_{cont} \approx 10^6$ N/m). The first error is usually compensated by calibrating the DMA apparatus before measurements, but the contact error cannot be avoided and leads to a significant lowering of the effectively measured Young's modulus Y_{eff} which for parallel-plate geometry is given as

$$Y_{eff} = k_{eff} \cdot \frac{h}{S} \qquad [\mathbf{2}]$$

$$\frac{1}{k_{eff}} = \frac{1}{k_{sample}} + \frac{1}{k_{cont}} \qquad [3]$$

where h and S are thickness and contact surface of the sample.

Details of the experimental setup may be found in refs. (*153, 154*).

Figure 11 displays the temperature dependences of the sample heights of pure Vycor and Vycor filled with salol. For these thermal expansion measurements no force is applied at all. As expected for pure Vycor h(T) decreases almost linearly with decreasing temperature, whereas the salol-filled sample shows a strongly nonlinear decrease of h(T) due to the vitrification of salol in the pores[1]. As already mentioned above, the glass transition temperature T_g of confined salol appears to be similar to the bulk value of ≈ 220 K.

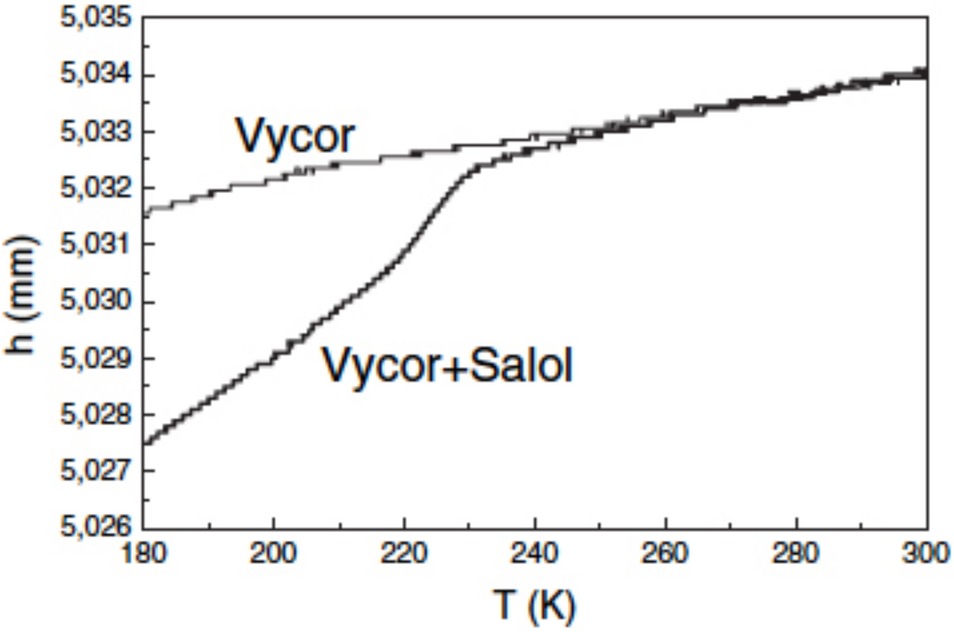

Figure 11: Sample heights h(T) measured for pure Vycor and Vycor filled with salol, normalized at 300 K.

---

[1] An estimation using the density data of liquid and solid salol *(186)* shows, that the observed length change must originate from about 20 vol% of salol material, which is in good agreement with the 28% porosity of Vycor. It implies that the measured response is due to the material inside the nanopores and does not result from residual material on the sample surface.

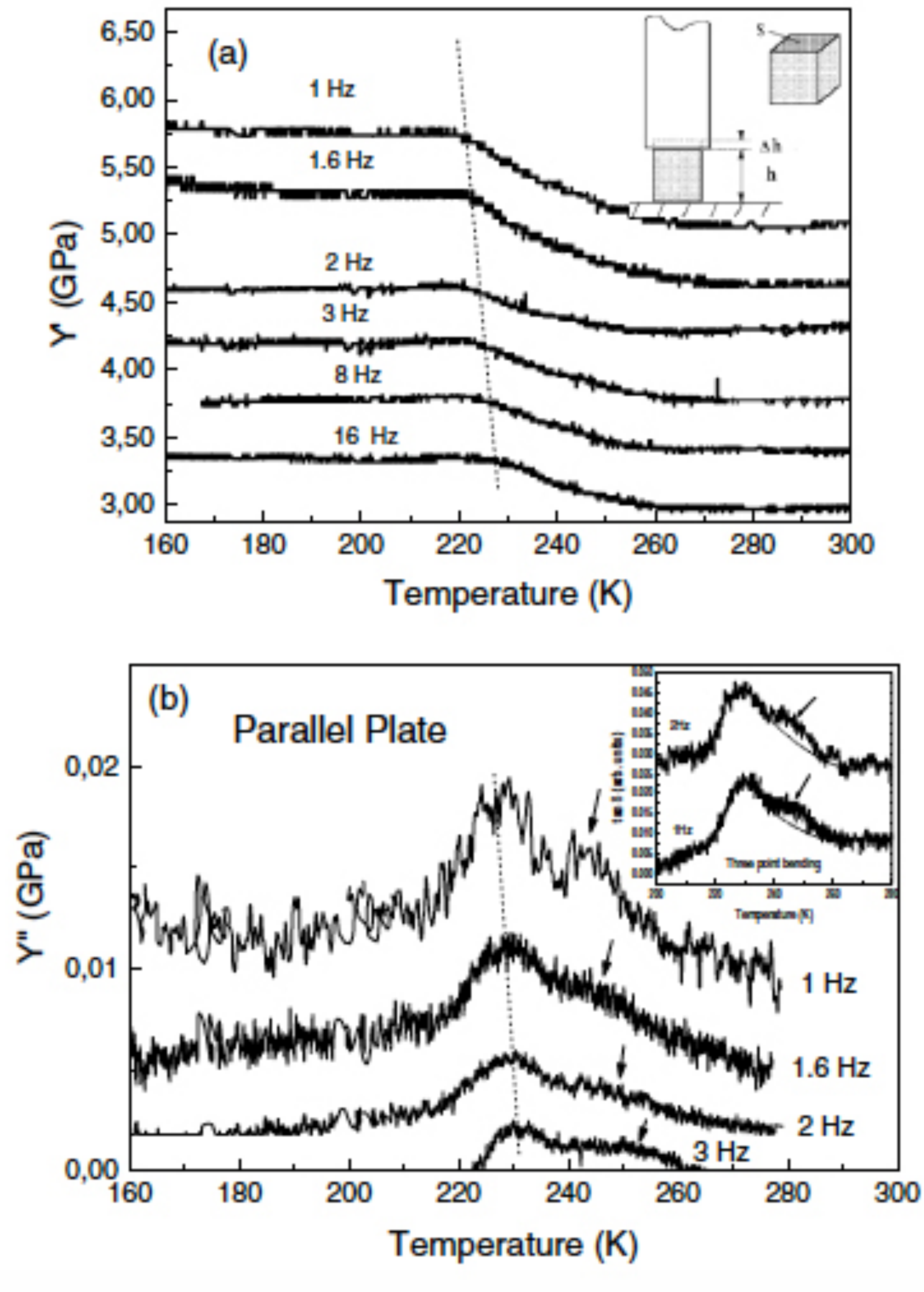

Figure 12: Real (a) and imaginary (b) parts of the complex Young's modulus of salol confined to Vycor glass (d = 7 nm) measured in parallel-plate geometry. The curves are offset from the 1 Hz data for sake of clarity. The inset shows typical results from three-point bending measurements.

Figure 12 gives an overview of dynamic parallel-plate measurements of salol confined to a Vycor glass of 7 nm-sized pores. The real (Y') and imaginary (Y'') parts of the complex Young's modulus $Y^* = Y' + iY''$ show several characteristic features, which we shall qualitatively discuss now before we present a detailed analysis of the data: As expected for a glass transition, with decreasing frequency the curves shift to lower temperatures. However the crossover region between the high- and low-temperature limits (relaxed and unrelaxed moduli) of Y' and Y'' appears to be rather broad (≈ 40 K). This also shows up in a rather big tail on the high-temperature side of Y', followed by an abrupt change on the low-temperature side, resembling a two-step (or double S-shaped) behaviour. In accordance with this the corresponding loss moduli Y'' show two rather broad peaks, which are separated by about 18 K in temperature. Three-point bending measurements which we have performed as a function of temperature for various measurement frequencies show the same type of behaviour (inset of Figure 12(b)). It should be noted, that pure Vycor displays no anomalies in Y' and Y''. Y' decreases linearly with decreasing temperature by about 2% in the whole covered temperature range and the loss modulus Y'' is negligible, small and constant.

3.3. Interpretation and Comparison with Experiment

Measurements of the elastic response to an applied dynamic stress is a widely used technique for studying the slowing-down of the dynamics when approaching the glass transition temperature in glass-forming materials (*155, 156*). The DMA technique was already successfully applied to study the glass transition in molecular glass-forming liquids both in bulk materials (*157*) as well as confined in porous media (*146*). A quantitative analysis of the elastic behaviour of composites can be done on various levels of sophistication (*146, 158*). Using a simple mixing model, one obtains for Young's modulus Y_C of the composite salol+Vycor for serial mechanical coupling of Vycor and salol

$$Y_c = Y_v C_v + Y_s C_s \qquad [\mathbf{4}]$$

where Y_v, Y_s are the Young's moduli of Vycor (SiO_2) and salol and $C_v = 0.72$, $C_s = 0.28$ are the corresponding volume ratios. For parallel mechanical coupling one obtains

$$Y_c = \left(\frac{C_v}{Y_v} + \frac{C_s}{Y_s}\right)^{-1} \qquad [\mathbf{5}]$$

Using the values for the elastic moduli of SiO_2 ($Y_V = 72.4$ GPa) and salol in the liquid ($Y_s = 2$ GPa) phase we obtain an estimation of Young's modulus of the composite at room temperature as 6 GPa < Y_c < 51 GPa. Taking into account the above-mentioned errors in eq. **[**3**]**, we obtain for the effectively measured Young's modulus of the composite 4.2 GPa < Y_c^{eff} < 11.5 GPa. Using eqs. **[**4**]** and **[**5**]** and the value of the elastic modulus of salol in the liquid and the solid phase ($Y_s = 5$ GPa) we obtain upper and lower bounds for the relative changes of the composite Young's modulus during vitrification of $0.02 < \frac{\Delta Y_c}{Y_c} < 0.13$. This estimation of the expected effect explains why the vitrification process of salol within the pores of Vycor can be so easily detected by DMA experiments. The measured relative changes of the Young's modulus of about 10–20% (Figure 12a) are well within the above-calculated limits. Interestingly enough very similar conditions (with respect to the elastic moduli ratios) appear for a quite different system, i.e. for the transition of water into ice. Here the bulk modulus changes from about 2.2 GPa in the liquid state to about 9 GPa for polycrystalline ice (*159*). In an early work Sellevold and Radjy (*160*) studied the freezing of water confined in porous Vycor by dynamical mechanical resonance measurements (300 Hz – 1600 Hz). Very similar to our case they find a substantial increase of Young's modulus up to 70% and an enhancement of internal friction associated with the freezing transition of capillary condensed water in the nanopores.

To explain the crossover from the liquid to the glass state of salol confined in Vycor, we made several attempts to describe our experimental findings: A simple Kohlrausch or Cole-Davidson function even with extreme stretching parameters do not reproduce our data at all. Even in case, where we can fit $Y^{'}$, the peak in $Y^{''}$ appears to be shifted at about 20 K higher than the measured one! In fact all attempts to fit our data with a single relaxation time failed. This led us to the assumption that the dynamical behaviour of salol in the pores requires an inhomogeneous model taking into account a radial space dependence of the relaxation time (Figure 10). In fact such a model was very recently applied to describe inelastic neutron scattering experiments of salol confined in nanoporous silica glass (Gelsil) (*104*). In order to fit their data of the scattering function at all measured temperatures, the authors assumed a shift of the Vogel-Fulcher temperature according to

$$\mathrm{T_0(r) = T_{00}(r)} + \left[\frac{\mathrm{k}}{\mathrm{R - r + r_p}}\right] \qquad [\mathbf{6}]$$

where $\mathrm{T_{00}}$ is the Vogel-Fulcher temperature of the bulk liquid, $\mathrm{R = d/2}$ is the pore radius and $\mathrm{r_p}$ is a so-called penetration radius, i.e. a distance beyond which it is very unlikely to find a particle of the fluid. Using a Vogel-Fulcher temperature dependence of the relaxation time $\tau = \tau_0 e^{E/[T-T_0(r)]}$, one obtains a dependence $\tau(r)$ on the position of a relaxing volume in the pore:

$$\tau(\mathrm{r, T}) = \tau_0 \cdot exp\left[\frac{\mathrm{E}}{\mathrm{T - T_{00}(r)} + \left[\frac{\mathrm{k}}{\mathrm{R - r + r_p}}\right]}\right] \qquad [\mathbf{7}]$$

In fact such a parametrization is consistent with recent results from molecular-dynamics simulations which predict an exponential dependence of the relaxation time when approaching the pore walls (*142*). In ref. (*141*) it was shown, that close to the surface of the pores the r-dependence of the relaxation time can be described by the empirical ansatz $\tau(r) \propto e^{\pm\Delta(T)/(R-r+r_p)}$, where the positive (negative) sign corresponds to systems with rough (smooth) surfaces (Figure 10).

To calculate the macroscopic dynamic elastic response we integrate the dynamic complex Young's modulus — which here we assume to be of Cole-Davidson type over the pore volume. The averaged and normalized real and imaginary parts of $Y^*(\omega\tau) \propto \frac{1}{[1+i\omega\tau(r)]^\gamma}$ then read

$$Y' = 1 - \frac{2 \cdot \Delta Y}{R^2} \cdot \int_0^R \frac{\cos\left[\gamma \cdot \arctan\left(\omega\tau(r,T)\right)\right]}{[1 + \omega^2\tau(r,T)^2]^{\frac{\gamma}{2}}}\, r\, dr$$

$$Y'' = \frac{2 \cdot \Delta Y}{R^2} \cdot \int_0^R \frac{\sin\left[\gamma \cdot \arctan\left(\omega\tau(r,T)\right)\right]}{[1 + \omega^2\tau(r,T)^2]^{\frac{\gamma}{2}}}\, r\, dr \qquad [\mathbf{8}]$$

Inserting eq. **[7]** into eq. **[8]** we have simultaneously fitted the frequency and temperature dependences of the real and imaginary parts of the complex Young's modulus (Figure 12).

The present model reproduces our measurement data excellently (Figure 13) with fit parameters $\gamma = 0.4$, $T_{00} = 155$ K, $E = 1750$ K, $\tau_0 = 10^{-11}$ s and $k = 25$ nmK. Broadband dielectric spectroscopy data (*161*) of salol in Gelsil of 2.5, 5 and 7.5 nm pore sizes where interpreted in terms of a two-states model with dynamic exchange between a bulk-like phase in the pore volume and an interfacial phase close to the pore wall. For the bulk-contribution and 7.5 nm pores the authors obtained $\tau_0 = 10^{-15}$ s, $T_0 = 177$ K and $E = 1416$ K. The relaxation time of the surface contribution was shown to be two orders of magnitude higher. Of course these parameters cannot be directly compared with ours, since their fits where obtained from different equations, but a numerical evaluation of eq. **[5]** with our set of parameters also yields $\tau\,(r = R)/\tau\,(r = 0) \approx 100$ in the temperature range covered by dielectric spectroscopy.

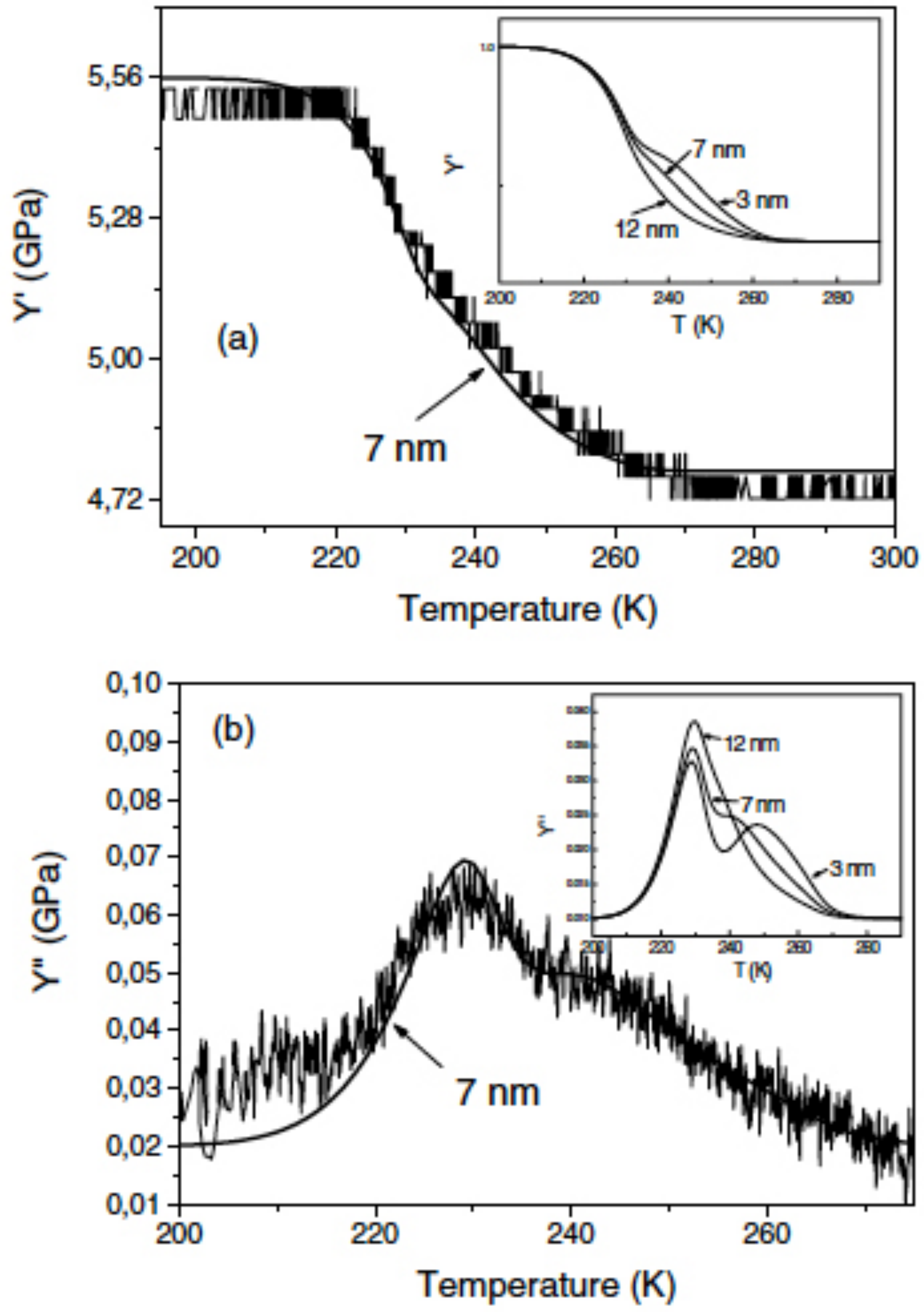

Figure 13: Fit of the dynamic (f = 1.6 Hz) elastic response of salol confined to 7 nm pores with the inhomogeneous model — eq. [8] — described in the text. The inset shows calculations with different pore sizes.

Very recently inelastic neutron scattering experiments of salol in Gelsil where performed (*104*). The authors used the same approach of inhomogeneous dynamics as we and obtained values of fit parameters for salol confined in 2.5

nm Gelsil: $\gamma = 0.322$, $T_{00} = 179$ K, $E = 831$ K, $\tau_0 = 10^{-13}$ s and $k = 5$ nmK. Unfortunately these parameters also cannot be directly compared to ours since the pore size, the host matrix and the measurement technique is rather different from ours. Moreover in a previous work it was shown, that the Vogel-Fulcher temperature can depend strongly on the low-frequency cutoff of the applied fitting range (*162*). Using dielectric and specific heat spectroscopy the author has shown, that the Vogel-Fulcher temperature T_0 can vary from 220 K to 140 K for frequency cutoffs between 10^{7} Hz and 10^{-3} Hz. This may explain the different T_{00} values obtained from inelastic neutron scattering and low-frequency Dynamic Mechanical Analysis. The other bulk values for salol reported in the literature (*161*) are $\tau_0 = 10^{-13}$ s and $E = 931$ K.

Interestingly in differential scanning calorimetry (DSC) measurements of salol confined to porous silica MCM-41 and SBA-15 a second anomaly at 14–16 K above the bulk glass transition was found (*136*). The authors interpret this additional specific-heat anomaly in terms of a second glass transition in the interfacial pore region. Our analysis of data, however, rather suggests, that the additional peak in the temperature dependence of the loss modulus Y'' is not related to the existence of a layer at the pore surface that is dynamically decoupled from the rest of the liquid, but is just the result of averaging over particles that have a distribution of relaxation times. A similar interpretation may also be appropriate for the additional specific heat anomaly of ref. (*136*). Indeed for increasing the pore size the present model yields a decrease of the second loss anomaly as well as a shift in temperature (inset of Figure 4), which very much resembles the findings of ref. (*136*).

Part of the above-mentioned complication, i.e. the increasing or decreasing T_g with varying pore sizes may originate from a transmission of surface-induced slowing-down or acceleration of molecules quite far into the pore volume. However salol seems to be a system, where the surface-induced slowing-down can be separated from the confinement-induced acceleration of the dynamics. Indeed in the framework of our model the extrapolated “core” Vogel-Fulcher temperature $T_0(r=0) = T_{00}+k/(R+r_p) \approx 160$ K, is about 35 K below the bulk value (194 K) measured by dielectric spectroscopy (*112*). It implies, that although the motion of molecules is slowed down near the rough surface of the pores, the relaxation times near the center of the pores are smaller at all temperatures compared to bulk salol. The present results for salol are consistent with the view that the α-relaxation is faster in confined geometries. Very recently Zorn et al. (*104*) arrived at the same conclusion from inelastic neutron scattering experiments of salol confined in nanoporous Gelsil with various pore sizes.

3.4. Conclusion

Summarizing, our measurements demonstrate, that Dynamic Mechanical Analysis provides a very sensitive method to test the dynamic behaviour of glass-forming liquids in confined systems. In favorable cases it allows to study the question, of whether or not there is an "intrinsic" size or confinement effect that is balanced by surface effects. Indeed the results of salol (inset of Figure 13) show, that for decreasing pore size the second anomaly in Y'' becomes more pronounced, making it easier to separate confinement and surface effects for the interesting case of pore sizes approaching the correlation length $\xi(T_g)$.

Experiments are under way to measure the glass transition dynamics of salol for various pore sizes of the host matrix.

ACKNOWLEDGEMENTS

Support by the University of Vienna within the IC Experimental Materials Science ("Nanostructured Materials") and the Austrian FWF (P19284-N20) is gratefully acknowledged.

Chapter 4

4. CONFINEMENT EFFECTS ON GLASS FORMING LIQUIDS

This chapter includes the manuscript of the published article "Confinement effects on glass forming liquids probed by dynamic mechanical analysis", *Physical Review B* 78, 054203 (2008) by J. Koppensteiner, W. Schranz and M.R. Puica (*84*).

“Confinement effects on glass forming liquids probed by dynamic mechanical analysis“, Physical Review B 78, 054203 (2008)

J. Koppensteiner, W. Schranz and M. R. Puica

Faculty of Physics, University of Vienna, Boltzmanngasse 5, A-1090 Vienna, Austria

ABSTRACT

Many molecular glass forming liquids show a shift of the glass transition T_g to lower temperatures when the liquid is confined into mesoporous host matrices. Two contrary explanations for this effect are given in literature: First, confinement induced acceleration of the dynamics of the molecules leads to an effective downshift of T_g increasing with decreasing pore size. Second, due to thermal mismatch between the liquid and the surrounding host matrix, negative pressure develops inside the pores with decreasing temperature, which also shifts T_g to lower temperatures. Here we present dynamic mechanical analysis measurements of the glass forming liquid salol in Vycor and Gelsil with pore sizes of d = 2.6, 5.0 and 7.5 nm. The dynamic complex elastic susceptibility data can be consistently described with the assumption of two relaxation processes inside the pores: A surface induced slowed down relaxation due to interaction with rough pore interfaces and a second relaxation within the core of the pores. This core relaxation time is reduced with decreasing pore size d, leading to a downshift of $T_g \propto 1/d$ in perfect agreement with recent differential scanning calorimetry (DSC) measurements. Thermal expansion measurements of empty and salol filled mesoporous samples revealed that the contribution of negative pressure to the downshift of T_g is small (< 30%) and the main effect is due to the suppression of dynamically correlated regions of size ξ when the pore size d approaches ξ.

4.1. Introduction

When approaching a glass transition some physical properties like viscosity or relaxation times change up to 14 orders of magnitude (*129, 130*). An explanation for the observed slowing down of the dynamics is the formation of collectively dynamically rearranging clusters (*18, 163*) or regions, with growing size ξ and increasing relaxation times as T_g is approached (*131*). The idea of an increasing dynamic correlation length ξ when approaching a glass transition is strongly supported by recent computer simulations (*143, 164, 165*), although not strictly proven, since computer simulations cannot treat the time range of the α-process. Very recently a breakthrough was achieved in this field. Biroli *et al.* (*166*) found first-time evidence that the mode coupling theory predicts a growing dynamic length scale approaching the glass transition of a supercooled liquid. The authors obtained a rather modest growth of the dynamical length scale ξ with decreasing temperature, which is in very good agreement with computer simulations (*143*) and experimental results. Indeed many experimental setups like heat capacity spectroscopy (*7, 167*), multidimensional NMR (*28, 29, 32*), multipoint dynamical susceptibilities (*21*), etc. have been used to monitor a possible growing length scale accompanying the glass transition. All these results agree in the fact that the obtained dynamically correlated regions - although material dependent - are of the order of 1-4 nm and display - if at all - a weak temperature dependence.

An alternative experimental approach to get a reference to a possibly existing cooperation length ξ which increases when $T \rightarrow T_g$ is by spatial limitation of a glass forming liquid. Spatially confining geometries as ultrathin films, mesoporous silica or zeolithes have already been used to study phase transitions of water (*168*), hydrocarbons (*169*), noble gases (*125, 170*), liquid crystals (*122*) or alkenes (*171*). But this concept also illuminated the old and still open question on the very nature of the glass transition and its dynamics (*128*): In a pioneering work Jackson and McKenna (*135*) studied the glass transition of organic liquids in controlled pore glasses (CPG) for various pore sizes d. They found a reduction of the glass transition temperature T_g for liquids in confinement as compared to the bulk material. The downshift of T_g was larger for smaller pore sizes, i.e., $\Delta T_g \propto 1/d$, an effect similar but not as strong as the suppression known for the melting temperature T_m in confinement. During the following two decades this effect was studied via calorimetry (*136, 172*), dielectric spectroscopy (*173*), neutron scattering (*104*), light scattering (*174*), and molecular dynamics (*141*). It was shown that in many cases confinement below a characteristic length impedes (*172*) the transition, implying that molecules within a region of the size ξ_g (approaching T_g typically some nm (*39, 175*)) have to cooperate and rearrange in order to create the glassy state. Hindering this cooperation first leads to a downshift of T_g if $d \sim \xi_g$ and finally to a suppression of the transition if $d < \xi_g$ (*172*).

However, although this shift of T_g with decreasing confinement size was found in numerous studies, there are complications which blur this simple picture: e.g. in many molecular dynamics simulations of glass forming liquids at high temperatures above the empirical mode-coupling temperature T_c confinement is found to slow down the dynamics (*176, 177*). Furthermore, in some systems a competition appears between slowing down of molecular motions due to pinning of the molecules at the pore surface and acceleration of the dynamics due to decreasing size of the confinement. Another effect occurs due to the difference in thermal expansion coefficients of the porous host matrix and the glass forming liquid. This may create negative pressure upon the confined liquid when the glass transition is approached. Some authors attribute the whole observed downshift of T_g to this negative pressure effect (*174*). We will address these points in more detail below. For excellent reviews about these topics the reader is referred to Refs. (*140*) and (*151*).

Very recently the confinement effect on the glass forming liquid salol was studied via dynamic mechanic analysis (DMA) measurements (*19*) in Vycor with d = 7 nm pore size. It turned out that the dynamic elastic response is very sensitive to the glass transition of liquids confined to mesoporous samples. Based on the results of computer simulations (*141, 142*) we could disentangle acceleration effects due to confinement and slowing down of molecular motion due to interaction of the molecules with the rough pore surface. We could even predict the pore size dependence of the dynamic elastic response (see Fig. 4 of (*19*) or Figure 13 of this work). In order to test these predictions and to study the glass transition of salol for different pore sizes, further measurements have been performed. Here we present experimental results of the temperature and frequency dependence of the complex dynamic elastic susceptibility of salol confined in mesoporous matrices of d = 7.5, 5.0, and 2.6 nm. In addition, thermal expansion measurements have been performed, which now allows us to take a new look at the often discussed negative pressure effect on glass forming liquids in confinement and to separate this effect from an intrinsic size effect.

The present paper is organized as follows: Section 4.2 yields insight into sample preparation and some technical details of DMA analysis. Section 4.3 displays a compilation of the experimental data and results of modeling and interpretation of the present data. It also contains a calculation of the effect of adsorption swelling and the separation of the actual downshift of T_g in salol into the negative pressure effect and the confinement effect. Section 4.4 concludes the paper.

4.2. Experiment

4.2.1. Sample Preparation

Porous Vycor samples are made by Corning Inc., NY and sold under the brand name "Vycor 7930". Via phase separation and leaching a three-dimensional random network of pores in nearly pure silica is fabricated (*88*). Pores are uniformly distributed in length, direction, and density (*89*). The mean ratio of average pore diameter d and pore length l, is $d/l \approx 0.23$. Gelsil is a mesoporous xerogel consisting of pure silica with a very narrow pore radius distribution. Gelsil rods were made by 4F International Co., Gainesville, FL. Results on pore sizes were derived from Barrett-Joyner-Halenda (BJH) analysis of the individual N_2-desorption isotherms (*178*) and are summarized in Table I:

Table I: N_2 adsorption characteristics of porous silica samples.

	Gelsil 2.6	Gelsil 5	Vycor
Av. pore diameter (nm)	2.6	5.0	7.5
Surface area (m^2/g)	586	509	72
Pore volume (cm^3/g)	0.376	0.678	0.214
Porosity φ	0.51	0.66	0.30

All samples were cut and sanded in order to gain parallel surface plains. The typical size of a sample was $(2\times2\times8)\ mm^3$ for parallel plate and about $(2\times1\times7)\ mm^3$ for three-point-bending DMA measurements. Cleaning was done in a 30% hydrogen peroxide solution at 90 °C for 24 h, drying at 120 °C in a high-vacuum chamber at 10^{-6} bar, also for about 24 h. The guest glass forming material was salol (phenyl salicylate, $C_{13}H_{10}O_3$), a low molecular weight liquid, whose melting temperature is $T_m = 316$ K. Salol is a standard, so-called fragile (*112*), glass former ($m = 73$) known (*136*) to form a glass either at extreme cooling rates of 500 K/min or in pores smaller than 11.8 nm. Filling was done at

317 K via capillarity wetting. By comparing the weight of clean and filled samples the filling fractions *f* were determined (see Table III).

4.2.2. Dynamic Mechanical Analysis (DMA)

In this method a static and a dynamic force $F_{stat} + F_{dyn} \cdot e^{i\omega t}$ (0.001 - 16 N at 0.01 - 100 Hz) are applied on a sample using a quartz or steel rod (see Figure 14). The response of the sample is measured via the displacement of the rod. Absolute height h, height amplitude Δh and phase lag δ are read via electromagnetic inductive coupling (LVDT) with a resolution of 10 nm and 0.01°, respectively. These data allow direct access to real and imaginary parts of the complex elastic susceptibility at low frequency and as a function of temperature and applied force. In addition, the thermal expansion of a sample can be determined in the so-called thermo mechanical analysis (TMA) mode, where no external force is applied. Two devices are used: A DMA 7 and a Diamond DMA, both from Perkin Elmer Inc. Two measuring geometries are applied: Parallel plate (PP) compression and three-point bending (3PB) (see Figure 14).

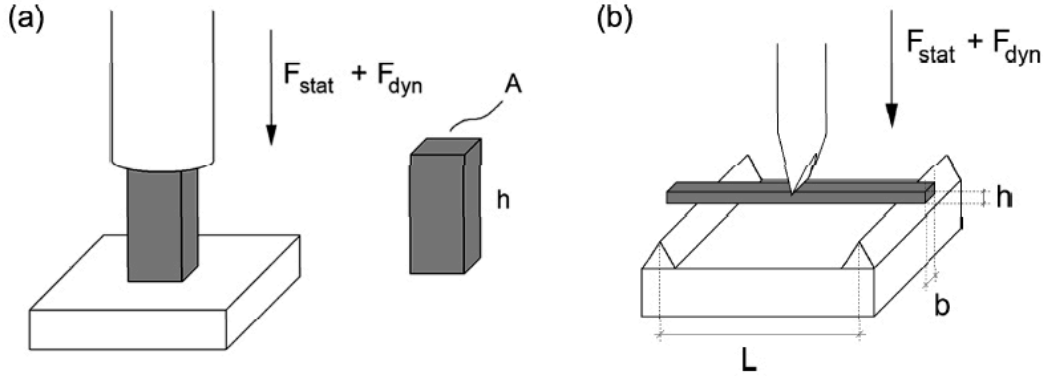

Figure 14: Sketch of (a) parallel plate and (b) three-point-bending geometry.

Parallel plate geometry reveals purely the complex Young´s modulus $Y^{*} = Y^{'} + iY^{''}$, where $Y^{'}$ and $Y^{''}$ are the storage and the loss modulus, respectively. The three point bending geometry delivers Young´s modulus plus a small (geometry dependent) contribution of a shear elastic constant. More details on measurement geometry may be found in Refs. (*153*) and (*154*). The absolute accuracy of resulting real and imaginary parts $Y^{'}$ and $Y^{''}$ is rather poor, mainly because of contact losses between the quartz rod and the sample. A discussion of these systematic errors may be found in (*19*). In contrast the relative accuracy is excellent and the DMA method is estimated to be about 100 times more sensitive to detect glass transitions or other subtle phase transitions than differential scanning calorimetry (DSC) measurements (*179*).

4.3. Results and Discussion

4.3.1. Dynamic Elastic Response

Diamond DMA measurements (in parallel plate and three-point-bending geometry) of Vycor and Gelsil samples filled with salol are shown in Figs. 15-18. The loss modulus Y'' [Figure 15(b)] of salol in 7.5 nm pores clearly shows a "two-peak structure", i.e., a peak with half-width at half maximum (HWHM) about 20 K, and a shoulder or second peak at about 15 K higher temperature [also see Figure 18(b)]. This is also reflected by the real part Y', which displays a "two-step-like shape" with temperature [Figure 15(a) and Figure 18(a)]. Both peaks in Y'' shift to higher temperatures with increasing frequency as expected for a glass transition. In smaller pores of Gelsil 5.0, peak and shoulder merge into one asymmetric peak of width ~ 30 K [see Figure 16(b) and Figure 18(e)], also shifted with higher frequency to higher temperatures. In 2.6 nm pores the loss peak shows a rather symmetric form broadened up to about 60 K [see Figure 17(b) and Figure 18(f)].

While in large pores of 7.5 nm diameter vitrification of salol seems to happen decoupled (two peaks in Y'') in regions near the pore surface and the pore center; things change in smaller pores. With decreasing pore diameter, Y'' approaches a symmetric form and simultaneously Y' changes from a "double step shape" into a "single step shape", indicating only one type of relaxation process. Similar broadening effects as for the loss peaks of our DMA measurements were observed in pores of decreasing size also by calorimetric (*135*) and dielectric measurements (*23, 180*). This broadening as well as a shift of the glass transition to lower temperatures was calculated by Sappelt and Jäckle (*181*) using kinetic Ising and lattice gas models, and shown to originate from confinement induced suppression of cooperative motion of molecules.

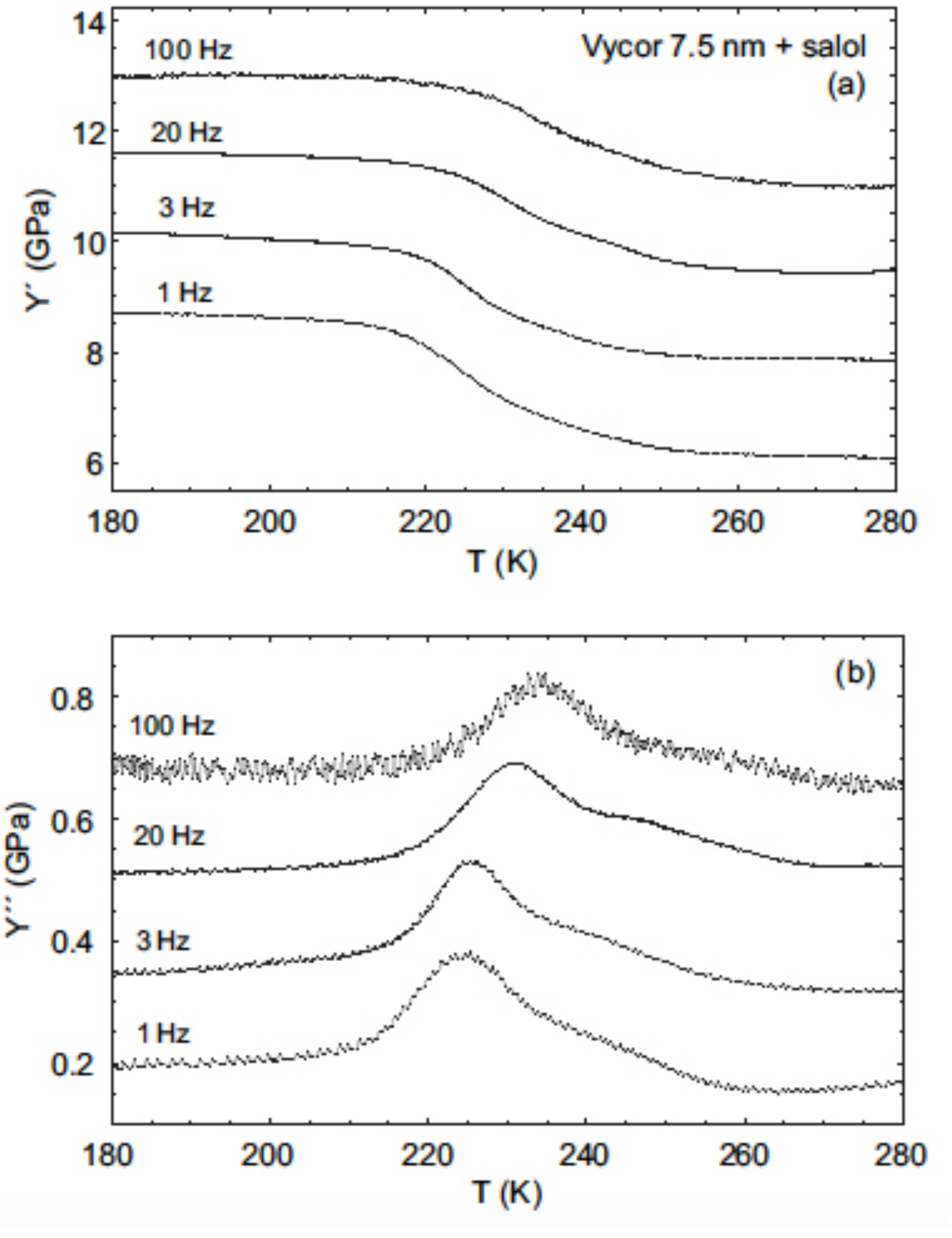

Figure 15: Real (a) and imaginary parts (b) of the complex Young´s modulus of Vycor 7.5 nm filled with salol (filling fraction f ≈ 0.79) measured in three-point-bending geometry. The curves are offset from the 1 Hz data for sake of clarity.

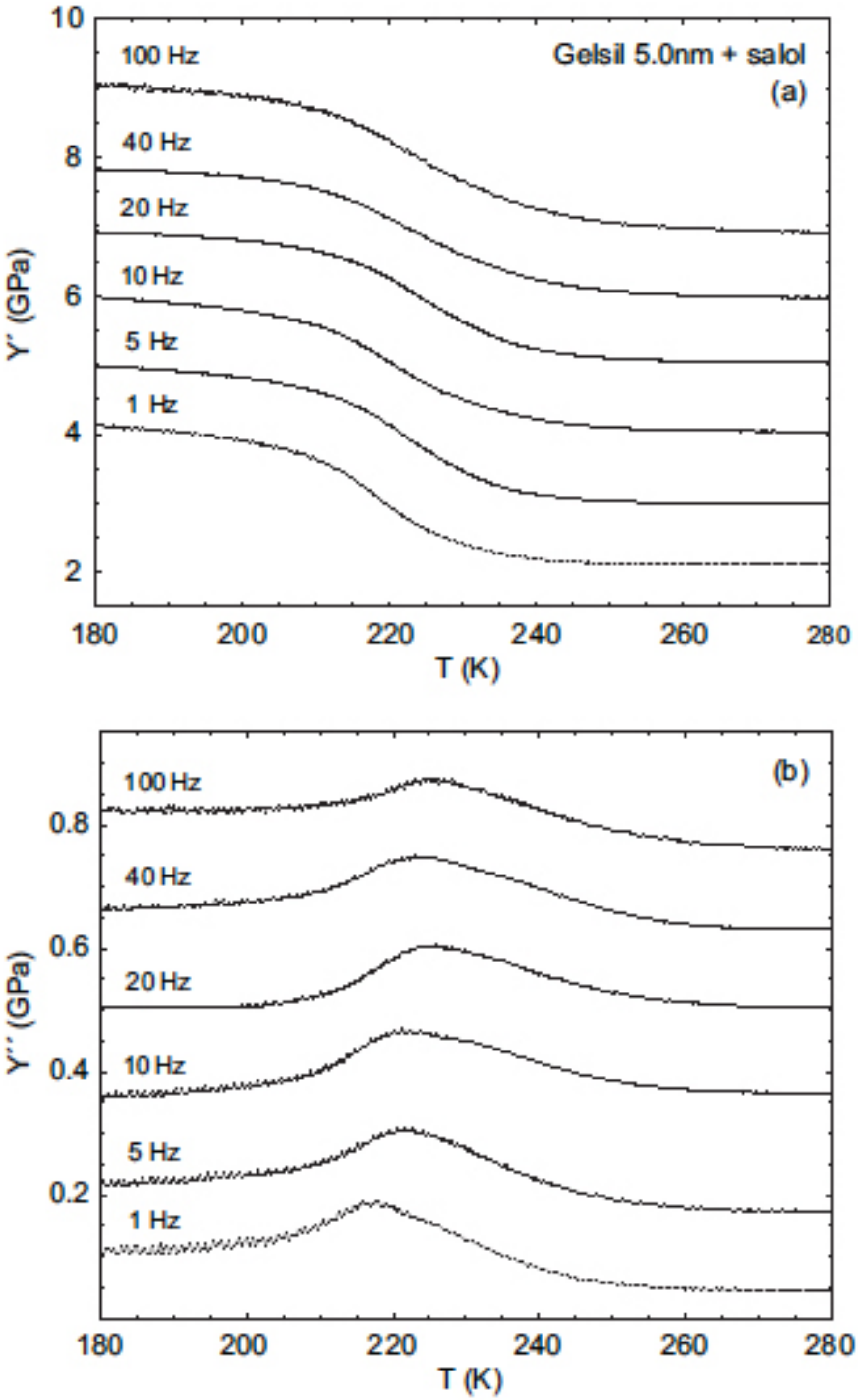

Figure 16: Real (a) and imaginary (b) parts of the complex Young´s modulus of Gelsil 5.0 nm filled with salol (filling fraction f ≈ 0.75) measured in parallel plate geometry (Diamond DMA). The 1 Hz signal is original data; other signals are offset for sake of clarity.

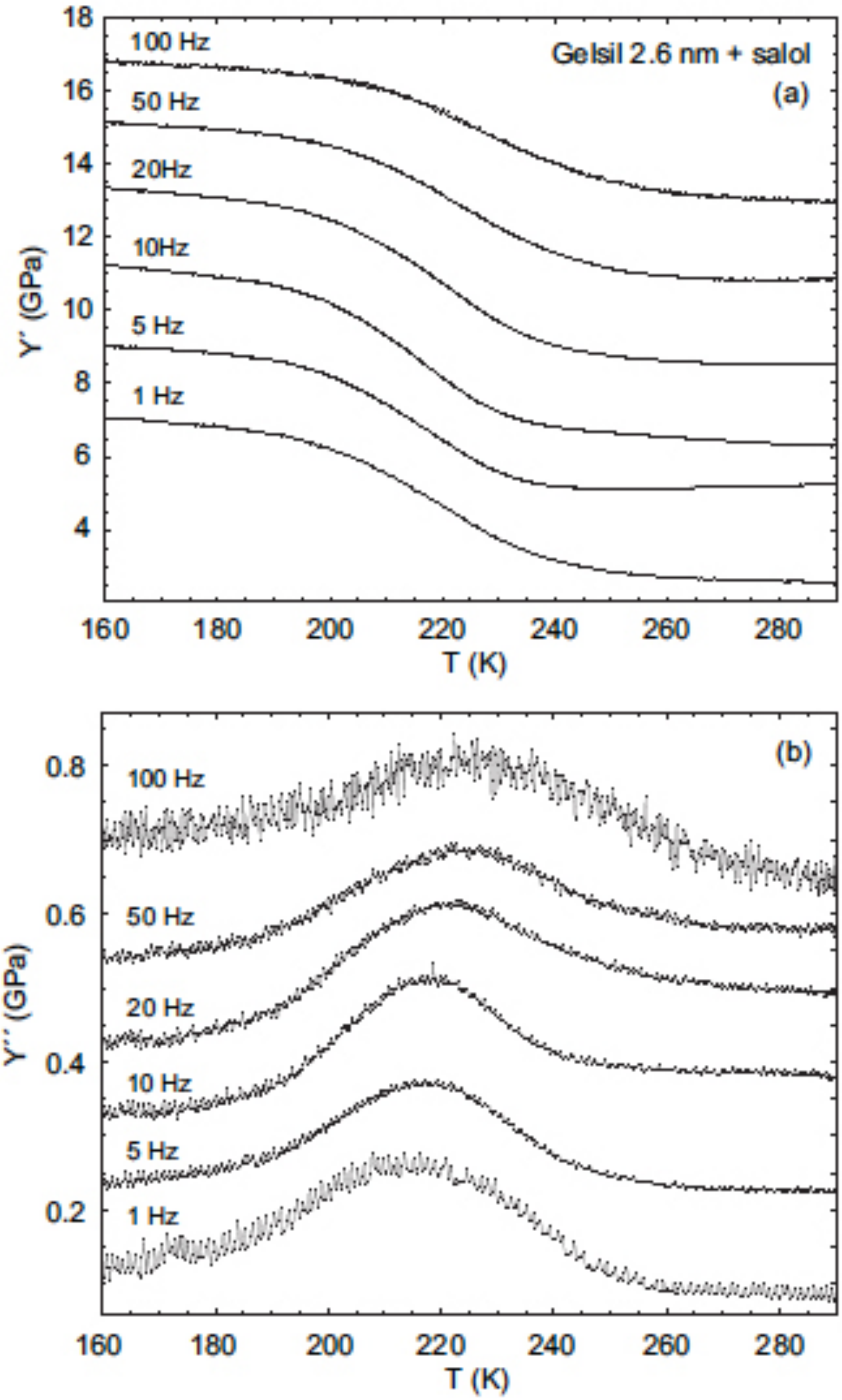

Figure 17: Real (a) and imaginary (b) parts of the complex Young´s modulus of Gelsil 2.6 nm filled with salol (filling fraction f ≈ 0.65) measured in three-point-bending geometry (Diamond DMA). The 1 Hz signal is original data; other signals are offset for sake of clarity.

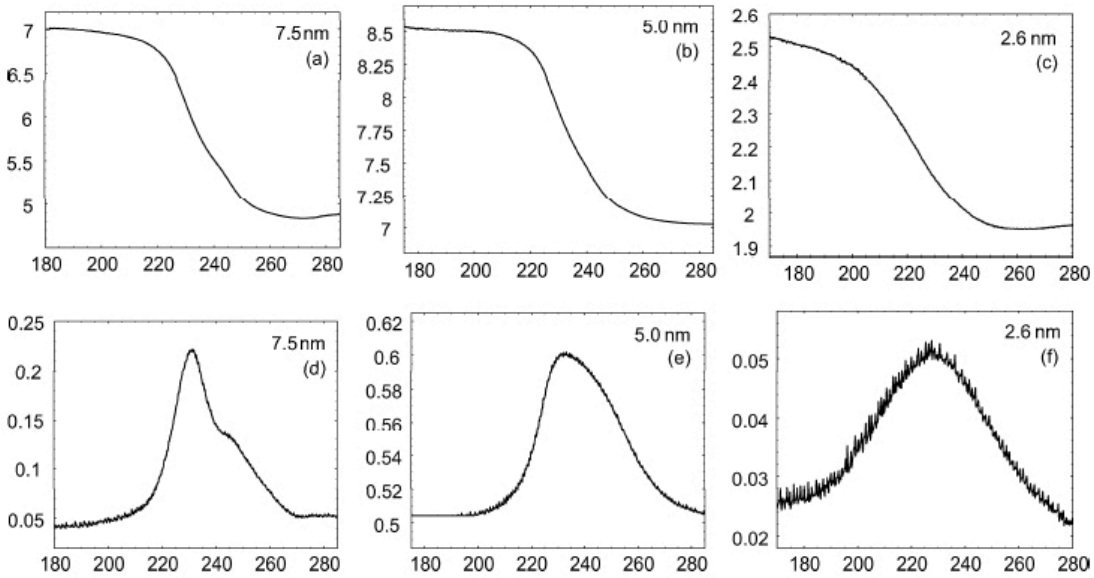

Figure 18: Real (a) and imaginary (b) part of the complex Young´s modulus of salol in Vycor or Gelsil for different pore sizes, all measured at 20 Hz.

Pure Vycor and Gelsil, meaning exposed to air and therefore mostly filled with nitrogen, do not show any of these features. Y' decreases about 2% between 300 K and 180 K. Y'' is constant within the corresponding temperature range.

Any standard relaxation model like Debye, Kohlrausch, Cole-Cole or Cole-Davidson fails to describe our dynamic elastic susceptibility data if only one type of relaxation process is assumed. One would have to use extreme stretching parameters to fit Y', which then leads to improper temperature shifts of the peaks in Y'' with respect to the experimental data and misfitting signal heights. The most efficient model to describe our data turned out to be a modification of the empirical Vogel-Fulcher-Tammann law

$$\tau(\mathrm{T}) = \tau_0 \cdot exp\left[\frac{\mathrm{E}}{\mathrm{T}-\mathrm{T}_0}\right] \qquad \textbf{[9]}$$

where τ_0 is a preexponential factor, $\mathrm{E}\cdot k_B$ is an activation energy, and T_0 is the Vogel-Fulcher (VF) temperature. Following computer simulations (*141, 142*) we take into account a shift of VF temperatures along the pore radius r . In a recent paper Zorn et al. (*104*) suggest the empirical ansatz

$$\mathrm{T_0(r)} = \mathrm{T_{00}(r)} + \left[\frac{\mathrm{k}}{\mathrm{R - r + r_p}}\right] \qquad \textbf{[10]}$$

with the bulk VF temperature $\mathrm{T_{00}}$, and the pore radius R=d/2. The so-called penetration radius $\mathrm{r_p}$ is the radius beyond which it is very unlikely to find a particle in the fluid state (*141*). The combination of Eqs. **[**9**]** and **[**10**]** leads to a radial distribution of relaxation times τ inside the pore:

$$\tau(\mathrm{r, T}) = \tau_0 \cdot exp\left[\frac{\mathrm{E}}{\mathrm{T - T_{00}(r)} + \left[\frac{\mathrm{k}}{\mathrm{R - r + r_p}}\right]}\right] \qquad \textbf{[11]}$$

Equation **[**11**]** describes the exponential increase in relaxation time when a rough pore wall is approached, and a growing influence of the pore wall with decreasing temperature, a behaviour which was also found by recent computer simulations (*141-144*). A temperature parametrized Cole-Cole plot of Y'' vs Y' of our data calls for a Cole-Davidson model of the complex dynamic elastic susceptibility

$$\mathrm{Y^*(\omega)} \propto \frac{1}{(1 + \mathrm{i}\omega\tau)^{\gamma}} \qquad \textbf{[12]}$$

with ω = 2πν, ν being the measurement frequency, and the broadening parameter γ. Using Eq. **[**11**]**, averaging over the pore radius R, and separating real and imaginary part of $\mathrm{Y}^* = \mathrm{Y}' + \mathrm{i}\cdot\mathrm{Y}''$ by common procedures leads to

$$\mathrm{Y}' = 1 - \frac{2\ \cdot \Delta\mathrm{Y}}{\mathrm{R}^2} \cdot \int_0^R \frac{\cos\left[\gamma \cdot \arctan\left(\omega\tau(\mathrm{r, T})\right)\right]}{\left[1\ +\ \omega^2\tau(\mathrm{r, T})^2\right]^{\frac{\gamma}{2}}}\ \mathrm{r\ dr} \qquad \textbf{[13]}$$

$$\mathrm{Y}'' = \frac{2\ \cdot \Delta\mathrm{Y}}{\mathrm{R}^2} \cdot \int_0^R \frac{\sin\left[\gamma \cdot \arctan\left(\omega\tau(\mathrm{r, T})\right)\right]}{\left[1\ +\ \omega^2\tau(\mathrm{r, T})^2\right]^{\frac{\gamma}{2}}}\ \mathrm{r\ dr} \qquad \textbf{[14]}$$

As already mentioned above, the two-peak structure in Y'' of 7.5 and 5 nm confined salol (Figure 15 and Figure 16) suggests to split the dynamic elastic response into a core and a surface contribution: The molecules in the core (center of the pores) behave bulk like and are dynamically decoupled from the molecules near the pore surface. This is modeled by inserting into Eqs. **[**13**]** and **[**14**]** the corresponding relaxation times $\tau_0 \cdot \exp[E/(T - T_0)]$ given by Eq. **[**9**]** if $r \leq R_C$ and $\tau(r,T)$ given by Eq. **[**11**]** if $r > R_C$ (see also Figure 20). The sum of the two contributions perfectly describes our Y' and Y'' data on salol in 7.5 and 5 nm pores simultaneously (see Figure 19).

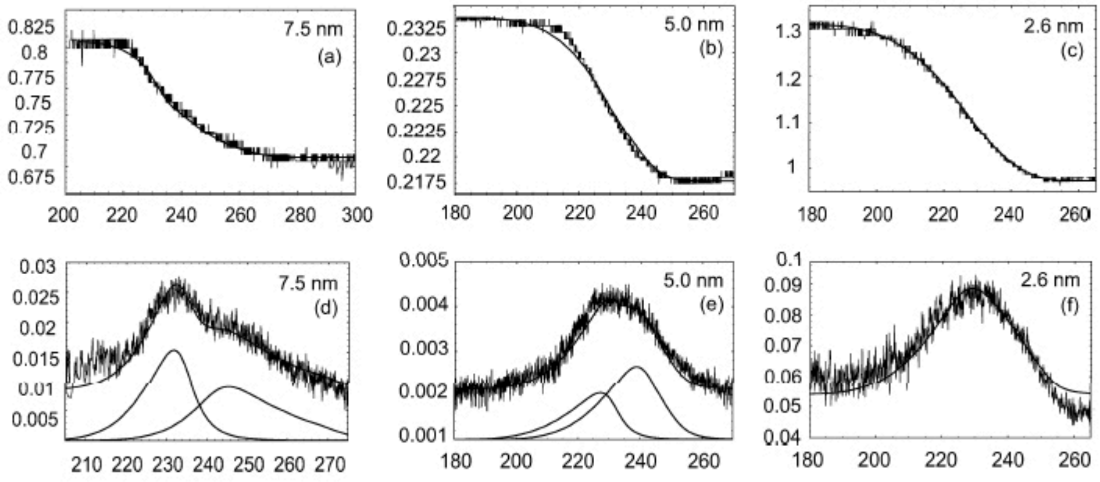

Figure 19: Real part Y' and imaginary part Y'' of different porous samples filled with salol. The lines are fits using Eqs. **[**13**]** and **[**14**]** with parameters of Table II.

In 2.6 nm pores we do not expect any molecule to behave like the bulk liquid any more, since the pore radius is of the same order as the estimated surface shell (see Table II), implying that every molecule is influenced by the near surface. Therefore we use Eqs. **[**13**]** and **[**14**]** with no bulk term which reproduces one single peak and also fits our data very well [Figure 18(c) and 18(f) and Figure 19(c) and 19(f)].

Table II: Fit parameters used in Eqs. [13] and [14] for fits of Figure 19.

	Vycor	Gelsil 5	Gelsil 2.6
R (nm)	3.75	2.50	1.28
r_p (nm)	0.36	0.25	0.28
E (K)	1750	1750	1750
T_{00} (K)	158.5	156.2	136.0
τ_0 (s)	10^{-11}	10^{-11}	10^{-11}
γ	0.33	0.18	0.15
K (nm K)	18	11	25
R_c (nm)	2.5	1.35	-
Shell $R - R_c$ (nm)	1.25	1.15	1.28

The radius of the "core" of bulk like interacting molecules turned out to be R_C = 2.5 nm and 1.35 nm in 7.5 nm and 5.0 nm pores, respectively (see Table II). This implies that the thickness of the shell of molecules being slowed down by wall interaction $R - R_C$ = 1.25 nm and 1.15 nm for 7.5 nm and 5.0 nm pores, respectively.

Additional loss peaks, attributed to molecules forming H bonds to the inner pore surface, have also been reported from dielectric measurements of salol in 7.5 nm pores (*22, 182*). The work of Kremer and Stannarius (*182*) also revealed that the typical size of a shell of molecules interacting with the pore surface is about 2 or 3 molecules. Since the size of a salol molecule is estimated as (1.4×0.6×0.4) nm^3 in (*183*) or as 0.282 nm^3 in (*184*), both corresponding to a mean diameter of 0.8 nm, this shell size is on the order of 1.6 to 2.4 nm. This is in very good agreement with our findings (see Table II). The core size R_C decreases with decreasing pore radius (see Table II and Figure 20), also in very good agreement with the results of Kremer *et al* (*173*).

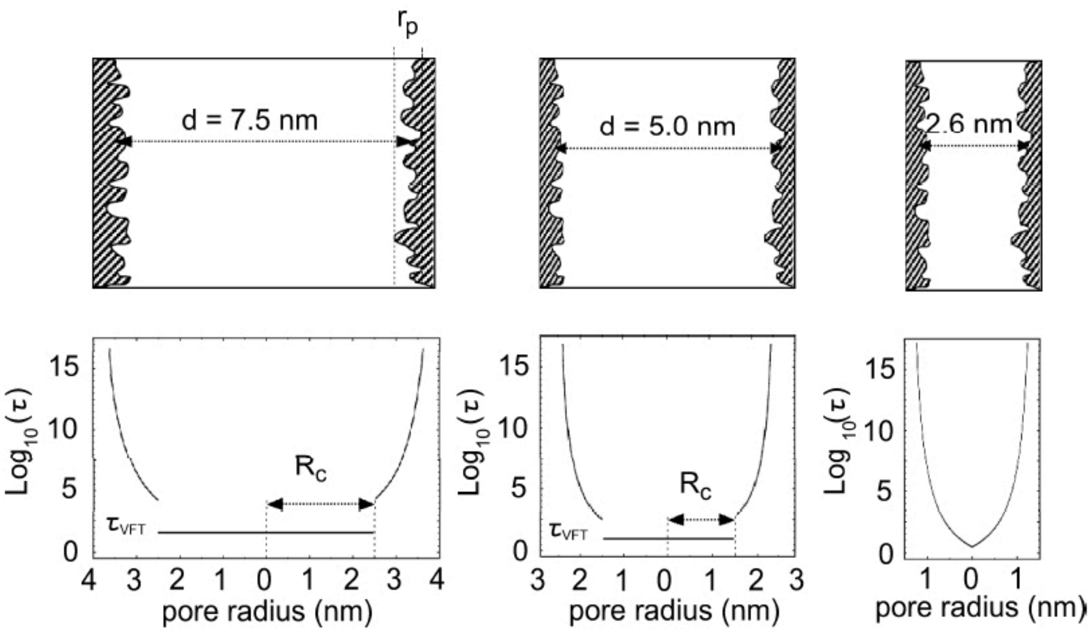

Figure 20: Modeled relaxation time distributions in pores of diameter 7.5 nm to 2.6 nm from Eq. **[**11**]** used in Eqs. **[**13**]** and **[**14**]** for fits of Figure 19.

The fitted Vogel-Fulcher temperature T_{00} is reduced with respect to the bulk and with decreasing pore size (see Table II). In order to compare our results with published data, we plotted the relaxation time in the pore center $\tau(r=0, T)$ for various pore sizes d and determined the corresponding $T_g(d)$ by using the common procedure (*184*) for finding the laboratory glass transition temperature, i.e., a cut with a horizontal line at τ = 100 s (see Figure 21). As shown in Figure 24, this leads to glass transition temperatures decreasing $\propto 1/d$ in very good agreement with published data of DSC measurements (*174*).

On the other hand there are molecular dynamics simulations (*176, 177*) of glass forming liquids pointing to the fact that at higher temperatures above the mode coupling temperature T_C = 260 K of salol (*185*) confinement slows down the dynamics. However within the present experimental frequency range (0.01-100 Hz) we are not able to detect such a crossover to confinement induced slowing down by heating the sample from T_g to temperatures above T_C for the following reason: An extrapolation of the relaxation times of Figure 21 to these temperatures shows that $\tau(T>260\ K) < 10^{-4}$ s, implying that $\omega\tau < 1$ within this temperature range even at the highest available measurement frequency of 100 Hz. Therefore the dynamic elastic susceptibility given by Eq. **[**12**]** is actually independent of τ and we have to extend our frequency range to higher frequencies. Work in this direction using resonant ultrasound spectroscopy (RUS, 50 kHz < ν < 1.5 MHz) is in progress.

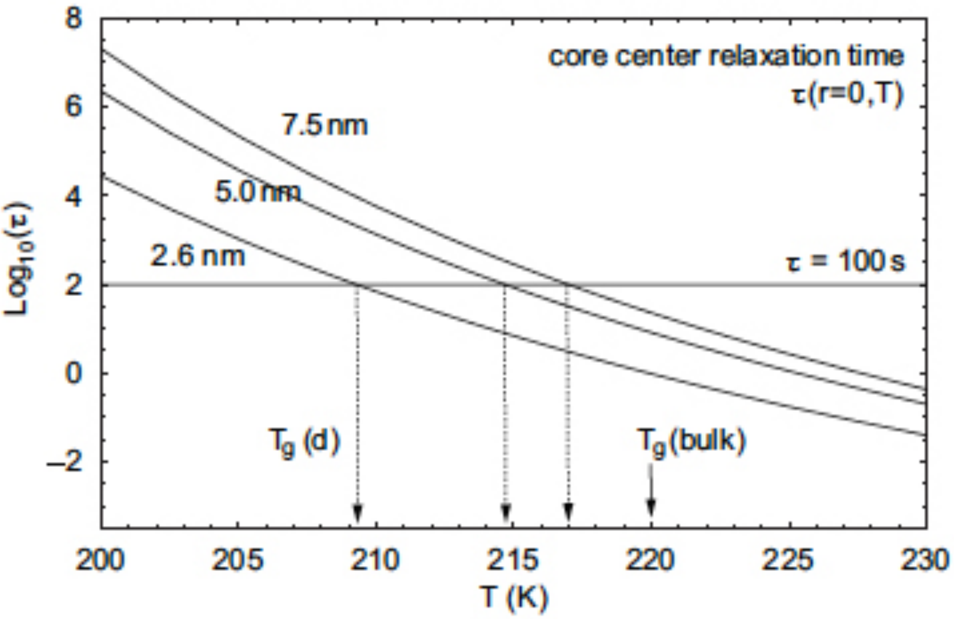

Figure 21: Relaxation time in pore centers calculated from Eqs. **[**9**]** and **[**11**]** with corresponding parameters from Table II. The horizontal line shows τ = 100 s.

4.3.2. Filling Process and Accompanying Effects

By using a DMA in a static TMA mode one can detect small changes in a sample´s height with a resolution of 10 nm. We measured the time dependent swelling of the Vycor and Gelsil samples during filling with salol and the thermal expansion of empty and filled samples in the following way: In parallel plate mode, the quartz rod is placed on top of the sample with force F = 0 N, and just height and temperature signals are read out. A clean piece of Vycor/Gelsil sample is cooled down to 170 K. Afterwards the sample is heated slightly above the melting temperature T_m = 316 K of salol and kept there isothermally. Crystalline, powder-like salol placed right around the sample melts and percolates the Vycor/Gelsil sample due to capillarity (Figure 22). After filling until saturation, the sample is cooled down to 170 K again (Figure 23). The time dependence of the filling process is displayed in Figure 22 for Vycor. While salol is percolating the sample, the temperature is held constant and the sample´s height is measured. Charts for Gelsil 5.0 nm and Gelsil 2.6 nm look very similar. The diagrams in all cases show the typical $\sqrt{t}$ behaviour as expected for a single capillary rise experiment, following Lucas (*186*) and Washburn (*187*). This result is in concordance with findings of Huber *et al.* (*188*), who investigated the mass uptake of porous silica samples and its time dependence, leading to the Lucas-Washburn $\sqrt{t}$ behaviour of the mass uptake with time. Very recently it was shown that the Lucas-Washburn equation (with small modifications) works well even at the nanoscale (*189*), which is in harmony with our results.

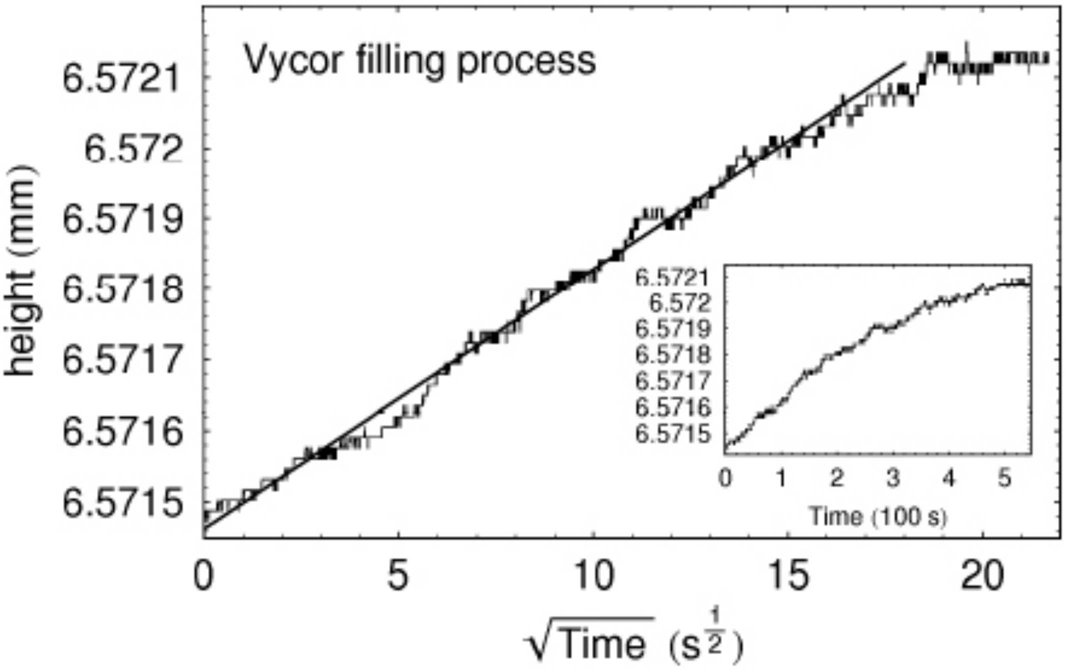

Figure 22: Height of Vycor sample during the filling process against $\sqrt{t}$. The inset shows sample height against time.

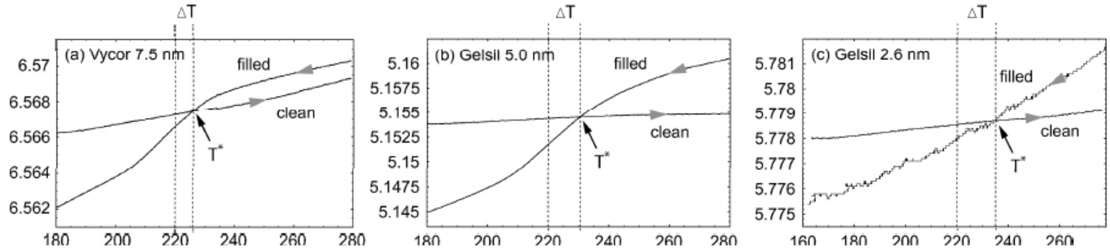

Figure 23: Linear thermal expansion of empty and salol filled samples with pore diameters of (a) 7.5 nm, (b) 5.0 nm, and (c) 2.6 nm.

The expansion of a porous sample during adsorption of gases or water has already been investigated in the 1920s (*190*). As a liquid/gas intrudes the sample it is subject to a negative hydrostatic pressure inside the pores, which leads to an expansion of the porous sample during adsorption of gases or water. Mesoporous media have enormous inner surfaces up to some 100 m^2/g (see Table I). This leads to a considerable stress reduction within the whole matrix and a sudden voluminal growth, which slows down and stops as all pore space is filled (see Figure 22). The change in height due to the adsorption swelling can even be calculated quantitatively. The pressure reduction of the liquid in a capillary is known (*191*) as $P_C = 2\sigma/r$, with the surface tension σ and the capillary radius r. With $\sigma = 1.73\times10^{-2}$ N/m from (*174*), this yields a capillary pressure of 26.6 MPa in 2.6 nm pores. This would lead to a hypothetical capillary rise of 1.8 km for salol. The linear strain $\epsilon = \Delta h/h$ accompanying the filling process can be computed by the equation (*192*):

$$\epsilon = \frac{f \cdot P_c}{3}\left(\frac{1}{K} - \frac{1}{K_s}\right) \qquad [15]$$

with the filling fraction f, the bulk modulus K of the empty host matrix, and the bulk modulus of the material building the solid frame K_S (which is nearly pure SiO_2). The bulk moduli K have been determined by RUS (*96*). Table III shows parameters used to calculate $\epsilon = \Delta h/h$. The calculated values for the adsorption swelling agree rather well with the experimental results.

Table III: Variables of Eq. **[**15**]**.

	Vycor	Gelsil 5	Gelsil 2.6
d (nm)	7.5	5.0	2.6
Porosity ϕ	0.31	0.66	0.51
P_c (MPa)	9.2	13.8	26.6
K (GPa)	8.1	3.9	9.6
f	0.77	0.62	0.32
ϵ_{calc}	2.3×10^{-4}	6.6×10^{-4}	2.2×10^{-4}
ϵ_{exp}	1.0×10^{-4}	4.1×10^{-4}	3.5×10^{-4}

4.3.3. Negative Pressure Effect

The downshift of the glass transition in nm-confining pores is often reported to obey a 1/d law [see (*135, 136, 174, 193*)]. At first this was proposed by Jackson and McKenna (*135*), following their former results on the shift of the melting transition T_m in confinement (*194*). But the supposed suppression of molecular cooperation when the pore diameter approaches an inherent length scale is not the only possible reason for a downward shift of T_g in confinement. Zhang *et al.* (*193*) proposed the increase in negative hydrostatic pressure within the pores due to mismatching thermal expansions of liquid and host matrix as the main driving force for the downshift of T_g. This idea was also discussed by Patkowski *et al.* (*174*) and Simon *et al.* (*195*), and was reviewed by Alcoutlabi and McKenna (*140*).

As Figure 23(a) shows, for large pores and in a cooling process starting at RT, at higher temperatures the Vycor matrix is not affected by its filling. It contracts like the empty Vycor matrix with a thermal expansion coefficient $\alpha = \Delta h/(h \cdot \Delta T) = 5.1\times10^{-6}\ K^{-1}$. Patkowski *et al.* (*174*) proposed the possible flow and equilibration of the confined liquid well above T_g, which we also consider to be the case here. But as vitrification sets in at about 230 K, the filled Vycor matrix is subject to a contraction which is stronger compared to the empty Vycor sample. Strong interaction (H bondings) between salol and the pore surface might be the reason for this. At smaller pores of filled Gelsil samples [Figure 23(b) and 23(c)] additional contraction already starts at higher temperatures. For an estimation of the process developing negative pressure upon the filling liquid, the strain misfit between the glass and the host matrix is

$$\Delta\epsilon^{\mathrm{mf}} = 3(\alpha_1 - \alpha_2)\Delta T \qquad \textbf{[16]}$$

with α_i, the thermal expansion coefficients of the host matrix (1) and salol (2). Negative pressure then derives from $\Delta P = \Delta\epsilon/\kappa_T$, where κ_T is the bulk compressibility of salol. The resulting shift of T_g, i.e.,

$$T_g\,(P) = T_g\,(P = 0) \cdot \left.\frac{\partial T_g}{\partial P}\right|_{P = 0} \cdot \Delta P \qquad \textbf{[17]}$$

crucially depends on the choice of ΔT, the temperature range, in which the effective negative pressure upon salol develops. This effective temperature range can be estimated from our data as follows: As calculated from Eq. [15] the host porous matrix expands with filling due to the negative capillary pressure which acts on the confined liquid. Since with cooling the liquid salol contracts, this stress relaxes and the composite is stress free if the filled sample height is the same as for the empty matrix which occurs at $T = T^*$ (see Figure 23). So $\Delta T \approx T^* - T_g$. Results of these estimations are given in Table IV. Parameters used for salol are $\kappa_T = 5\times10^{-10}$ Pa^{-1} from (*196*), the thermal expansion coefficient $\gamma_1 = 3\alpha_1 = 7.36\times10^{-4}$ K^{-1} from (*129*), and $\partial T_g/\partial P = 0.204$ K/MPa from (*197*). Our measurements are in accordance with enthalpy recovery results of Simon *et al.* (*195*). Their model shows that effective negative pressure develops 2 to 2.5 K above the reduced glass transition for samples with 11.6 and 25.5 nm pore sizes. Further, they state "...If negative pressure were the cause of the depressed T_g, the temperature at which isochoric conditions are imposed would have to be ~20 to 40 K above T_g." For comparison we obtain a necessary $\Delta T = 10$ to 40 K for d = 7.5 to 2.6 nm pores, which is in very good agreement with Simon *et al.*

In our opinion our calculated ΔT^{np} is still overestimated for two reasons: First, using the bulk value α_2 of the host matrix from Figure 23 does not take into account internal pore walls being affected by the negative pressure inside, relaxing to some extent and so reducing pressure. Second, thermal expansions of other glass forming liquids, e.g., toluene have been reported 1.5 times smaller in confinement (*198*) compared to bulk. Moreover, thermal expansion of liquid salol drops (*129*) to a *quarter* of its value at the glass transition. So, as the glass transition sets in, α_1 starts to decrease and a purely pressure induced downshift ΔT_g would be even more diminished. Apart from this the reason for the size dependence of the thermal mismatch effect (see Figure 24, open circles) is not clear at all.

Table IV: Parameters of ΔT_g estimations, $\Delta T_g^{exp} = \Delta T_g^{np} + \Delta T_g^{conf}$

	Vycor	Gelsil5	Gelsil2.6
d (nm)	7.5	5.0	2.6
α_2 (K^{-1})	$2.1 \cdot 10^{-5}$	$4.6 \cdot 10^{-5}$	$1.1 \cdot 10^{-5}$
ΔT (K)	6	10	15
$\Delta\epsilon^{mf}$(%)	−0.40	−0.60	−1.06
ΔP (MPa)	−8.1	−12.0	−21.1
ΔT_g^{np}(K)	−1.6	−2.4	−4.3
ΔT_g^{conf}(K)	−1.4	−2.9	−6.4
ΔT_g^{exp}(K)	−3.0	−5.3	−10.7

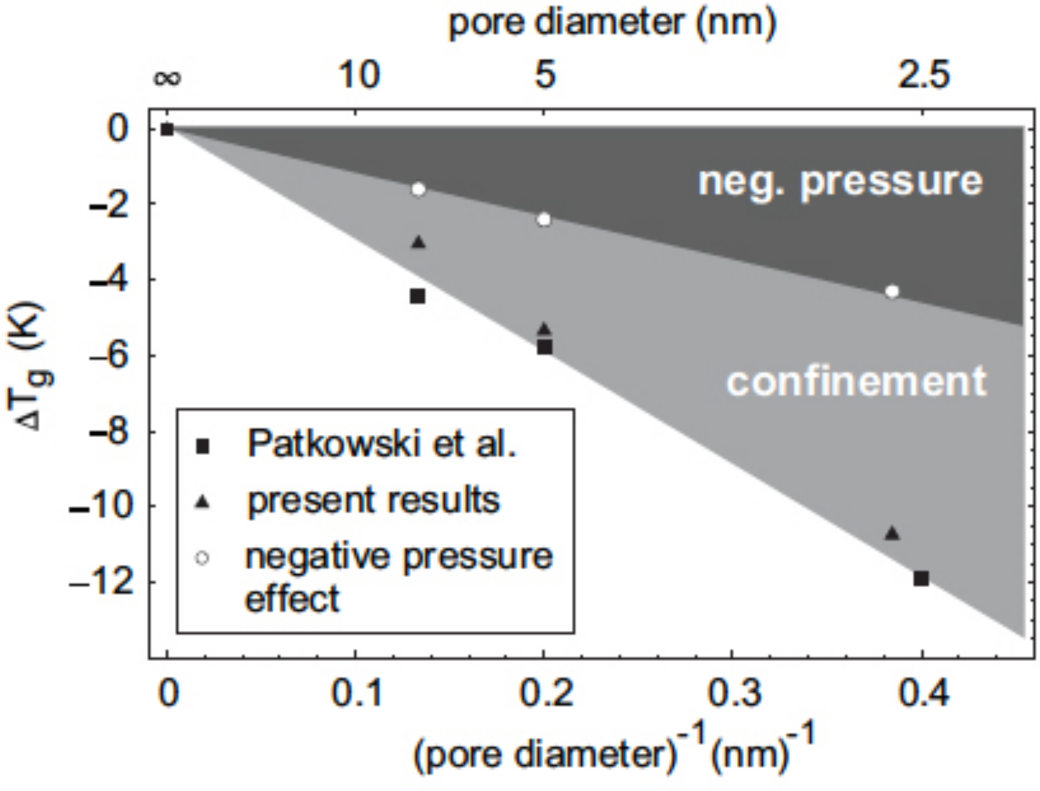

Figure 24: Shift of glass transition temperature against (pore diameter)$^{-1}$. The boxes are T_g's from Figure 21, triangles show literature values from (*174*), and open circles display the maximum negative pressure contribution (see section 4.4).

4.4. Conclusions

The glass transition of salol confined to porous host matrices of Vycor and Gelsil with pore sizes of 7.5, 5.0 and 2.6 nm has been measured by Dynamic Mechanical Analysers (DMA 7 and Diamond DMA, Perkin Elmer). The dynamic complex elastic susceptibility data can well be fitted assuming two types of dynamic processes: A "bulk" relaxation in the core of the pores and a radially increasing "surface relaxation" of molecules near the pore surface. The calculated core relaxation time shows a typical Vogel-Fulcher temperature dependence and decreases with decreasing pore size d. This confinement induced acceleration of dynamics leads to a shift of the glass transition temperature $T_g \propto 1/d$, which is in perfect agreement with recent DSC results (*174*). Measurements of the sample height with filling (adsorption swelling) and thermal expansion are used to calculate the effect of "negative pressure" due to thermal mismatch between the porous host matrix and the glass forming liquid. Such negative pressure could at least partly explain a shift of T_g in confined glass forming liquids (*140, 174, 195*). Our data show that for salol this effect of thermal mismatch could describe at most 30% of the observed downshift of T_g, which is in harmony with enthalpy recovery experiments (*195*).

In our opinion the main cause for the shift of T_g is a hindering of cooperativity due to confinement. This is also supported by an estimation of this effect using the results of Hunt *et al.* (*199*). They calculated the finite-size effect of the glass transition from percolation and effective medium models, which yields

$$T_g\,(d) = T_g\,(\text{bulk}) - \frac{0.5 \cdot E}{\ln\left(t \cdot \nu_{ph}\right)} \cdot \frac{r_0}{L} \qquad \textbf{[18]}$$

Inserting t = 100 s, $\nu_{ph} = 1/\tau_0$, and our fit parameters from Table II, and assuming that the typical distance between molecules r_0 is about the diameter of a salol molecule (*200*) ($d_0 \approx 0.8$ nm), we obtain ΔT^{Hunt} as 3.2, 4.8 and 9.1 K for 7.5, 5.0 and 2.6 nm pores, respectively. These calculated values agree surprisingly well with the measured confinement induced downshifts of T_g (d) (see Figure 24 and ΔT^{exp} in Table IV).

Moreover Eq. **[**18**]** predicts (*199*) that the size dependence of ΔT_g increases with increasing fragility (*113*),

$$m = \frac{E \cdot T_g}{\ln(10) \cdot \left(T_g - T_0\right)^2} \qquad \mathbf{[19]}$$

since m ∝ E. Indeed, this correlation between $\Delta T_g(d) \sim m$ was verified experimentally for many systems, i.e., for glycerol (*193*) (m = 53) ΔT_g (d = 2.5 nm) ≈ −4 K, benzyl-alcohol (*135*) (m = 65) ΔT_g (d = 2.5 nm) ≈ −9 K, salol (*174*) (m = 73) ΔT_g (d = 2.5 nm) ≈ −11 K, o-terphenyl (*174*) l (m = 81) ΔT_g (d = 2.5 nm) ≈ −25 K.

We think that these considerations, i.e., the downshift of T_g calculated via percolation theory, as well as the clear correlation between the magnitude of induced T_g shift and the fragility of a glass forming liquid, both confirm our other findings (see Figure 24) that the main effect of the confinement is to suppress cooperative motion. Negative pressure effects although always present contribute only little.

ACKNOWLEDGEMENTS

Support by the Austrian FWF (Grant No. 19284-N20) and by the University of Vienna within the IC Experimental Materials Science ("Bulk Nanostructured Materials") is gratefully acknowledged. We thank Marie-Alexandra Neouze and the Institute of Materials Chemistry from the Vienna University of Technology for the N2-characterization of our samples. We are grateful to J. Bossy (CNRS Grenoble) for supplying us with Gelsil samples.

Chapter 5

5. SUBSEQUENT APPLICATIONS

Our original contributions to the field (*19, 84*), published in the articles presented in the previous two chapters, have been cited by multiple studies since they appeared in print. This chapter reviews some of these subsequent applications and extensions of our work, as well as various models to analyze the experimental data, and alternative experimental techniques.

The DMA experiments described in chapters 3 and 4 were carried out on phenyl salicylate (salol, $C_{13}H_{10}O_3$) (*19, 84*). A similar approach has been employed subsequently for the study of other glass-forming liquids, ortho-terphenyl (OTP, $C_{18}H_{14}$) and methylbenzene (toluene, $C_6H_5CH_3$) (*201*). DMA of OTP in mesoporous confined systems revealed a downshift in T_g upon decreasing the pore size, in very good agreement with previously published reports (*135, 136, 140, 174*). Using a different method, NMR, showed that toluene exhibits a strong (37 K) upshift in mesoporous confinement (in 2.4 nm pores), presumably due to a strong interaction between its molecules and the surface (*139*). A qualitatively similar, but less strong upshift, was recently detected by DMA for toluene in nanoporous Gelsil and Vycor silica glass matrices (*201*). A comparable non-monotonic variation in T_g and consistent variations in molecular dynamics were also reported for other glass-forming liquids, including glycerol (*136*), benzene (*139*), polypropylene-glycol (*134*), methanol (*202*), and m-toluidine (*203*).

However, it is worth mentioning that the behaviour of a given material was found to depend substantially on the experimental conditions (or on the molecular dynamics simulation conditions) – i.e., under different conditions, T_g was observed to increase, decrease, remain constant, or even to disappear (*136, 139, 140, 193, 194, 204, 205*). Taking into account the very large number of experiments that were performed in the field, this testifies to the complexity of the issue at hand and reveals why a coherent and consistent interpretation of the obtained experimental data is not at all simple (*203*). Whereas numerous confinement experiments indicate a reduction of T_g as the pore size decreases (*96, 161, 206, 207*), as mentioned above, and in many cases with T_g changing inversely proportional to the pore diameter as first described in materials with a low molecular weight (*135*), reaching a conclusion on the growing cooperative length is not straightforward, given the various interfering, complicating mechanisms (*203*). Some effects that influence the dynamics vary with the physical or chemical properties of the confining material, which explains why the dynamics was found to slow down in confining media, as the "hard wall" can strongly hinder some of the molecules (*198, 203*). This is also seen in simulation studies, which reveal a slowing down of the relaxation dynamics by several orders of magnitude in the vicinity of a "rough wall" and the opposite effect, of dynamics speeding up when the pore wall is "smooth" (*142, 202, 208*). Molecular motions are also known to be slowed down appreciably because of adsorption effects at the walls (*209-211*). Despite these and other complicating factors (*212*), however, support for the inherent length scale and for the growing length scale upon lowering the temperature towards T_g is also provided by both experimental approaches – using techniques such as differential scanning calorimetry (DSC) (*7*) or multidimensional NMR (*32*) – and molecular dynamics simulations (*141, 165, 213*).

For our DMA analysis of salol confined into matrices of Gelsil and Vycor, the pores in the respective matrices were used uncoated or untreated (which are also known as "natural pores") (*19, 84*). An obvious extension of our work involves studying the behaviour of the same glass-forming material, salol, filled into mesoporous Gelsil and Vycor matrices with silanated pore surfaces (*81, 96*). These experiments were also performed using various pore sizes (between 2.4 and 7. 5 nm, similar to those used by us (*84*)), over a frequency range of 1 - 100 Hz. Compared to the original results, in this case silanation causes a complete removal of liquid-surface interactions, and consequently of surface-induced retardation of the molecular dynamics, and therefore produces a distinct enhancement, i.e. acceleration, of the dynamics. Moreover, under these conditions T_g decreases even more strongly with decreasing pore size, due to this lubrication effect, and consequently due to removing the surface-induced slowing down of molecular dynamics. Remarkably, these results enable one to distinguish between the side effects on the molecular dynamics, such as negative pressure and surface bondings, and the actual confinement effect, and to quantify these effects separately.

As discussed in the previous section, we detected two different glass transitions for salol confined in Gelsil and Vycor with pores larger than 5 nm in size, attributed respectively to a core (pore center, with bulk-like behaviour) contribution and to a surface contribution (*84*). In many other systems two glass transitions have been reported under confinement (*150, 161, 214, 215*). The transition with the lower T_g corresponds to the core regions, whereas the transition with the higher T_g corresponds to the regions near the pore surface, where the mobility is restricted by surface interactions. Interestingly, one finds the reverse geometrical case when investigating the dynamic elastic response in polyurea (a spontaneously occurring polymer-nanoparticle composite) when the volume fraction of the so-called hard nanodomains is small enough (≤ 12%). This happens because, in this case, these elastically hard nanodomains (microphase segregated hard segments) are embedded in the elastically compliant matrix (*3*). Such polymer-nanoparticle composites have also been reported to exhibit two different glass transitions (*216*). For microphase segregated polyurea networks, the transition with the lower T_g is thought to occur in the soft matrix, whereas the transition with the higher T_g at the interface between this matrix and the hard nanodomains (*3*). Since, as mentioned above, silanation removes liquid-surface interactions, the possible transition in the shell layer disappears, and only one glass transition process is observed (*81, 96*). This could indicate that the interactions at the surface of the pore are reduced by silanation, e.g. formation of hydrogen bonds (*102*), as seen in the case of diglycidyl ether of bisphenol A, an epoxy resin, filled into silica glasses with controlled pores with diameters in the range of 4 - 111 nm (*212*).

It is common to describe the behaviour of a pore-confined fluid using two components, a slower one and a faster one; this was applied to polymers (*217*), as well as other small molecules confined in silicon- or silica-based matrices (*126, 209, 218-221*). This translates into a thermodynamic partitioning of the condensate between a bulk, or core, phase component and a film-condensed component, the shell phase, characterized by strong interactions with the walls of the pore – and a corresponding partitioning of the mobility (*222*). However, this approach has been criticized as possibly too simplistic, given that even for small molecules the interaction potentials decay gradually with the distance between the respective molecule and the walls of the pore, thus suggesting a gradient in the molecular mobility over the distance between the wall and the center of the pore, rather than two distinct values (*202, 222*). Consequently, this would argue against the widespread method of separating the molecular mobility into a shell and a pure core molecular mobility, i.e. the so-called "two-state" or "two-layer" model (*84, 150, 223-225*). An alternative model was proposed based on the behaviour of salol confined in native sol-gel glasses (*22, 161*). This model assumes a dynamic exchange between molecules attracted to the walls of the pores and the core molecules affecting the overall dynamics of the confined molecules. Last, but not least, a "three-layer" model was proposed last year, based on results from calorimetric experiments in which three different glass transitions were detected in the poly(methyl methacrylate) polymer confined in nanopores (*226*).

Beside the porous media mentioned thus far (such as silica-based Gelsil and Vycor, and polyurea), a wide range of nanoporous materials have been used to study the behaviour of confined fluids and solids (*222*); these materials can be based on silicon (*227-232*), alumina (*233-235*), carbon (*236, 237*), gold (*238, 239*), or titanium (*240, 241*).

Most recently, the molecular dynamics, glass transitions, and crystallization kinetics of salol in confinement in porous uniaxial anodic alumina oxide membranes (AAO membranes) have been studied using dielectric spectroscopy and DSC (*105, 242*). These techniques revealed that upon increasing the geometrical confinement, T_g shifts toward lower values, while the structural relaxation shape broadens (*105*). As discussed above, these changes were attributed to the difference in molecular dynamics between the salol molecules located at the pore walls and the molecules in the center of the pore. Moreover, it was hypothesized that variations of the packing density of molecules located in the center of the pore contribute to a supplementary confinement effect, thus enhancing the structural relaxation dynamics (*105*). This is supported by previous results showing that substantial differences in both the structural relaxation and T_g can be induced by only a slight variation in the packing density within the pores (*174, 243*).

During the studies on the glass transition of salol confined in AAO membranes (*105*), the authors noticed that this glass-forming liquid undergoes a crystallization process at lower cooling rates, leading them to investigate the kinetics of crystallization and melting behaviour of salol (*242*). Their findings show that the kinetics of crystallization is dependent upon the degree of confinement, i.e. upon the pore diameter, and moreover as the pore size is reduced (e.g., to 13 nm), crystallization can even be completely suppressed. A result reminiscent of our findings on the dependence of T_g upon pore size (*84*) revealed that as the pore diameter is reduced, the melting point shifts towards lower temperatures (*242*). Similar studies, performed on confined benzene, confirm that on this scale crystallization is a complicated process, not unlike the glass transition. These studies concluded that the pore geometry also determines the crystallization process: the melting point occurs at a significantly lower size in slit pores than in cylindrical pores (*139, 244*). The energy related to salol nucleation and crystal growth, as well as the orientation of the crystals all vary with the pore diameter (*242, 245*). This reflects either a difference in the tendency for crystal growth under confinement, or the interaction between guest molecules and the host matrix being involved in the development of a negative pressure (*242*). The impact of the negative pressure on the measured T_g and on the molecular dynamics was also assessed in confined salol (*174*). Interestingly, while the negative pressure is important in regulating the dynamics of confined salol in AAO membranes, its influence on the crystallization process of confined salol is negligible (*105, 242, 246*).

Chapter 6

6. CONCLUSIONS

The present thesis begins by defining the glass transition and its characteristic temperature, T_g, after which it introduces a number of techniques that have been employed to measure this parameter. The second chapter presents our method of choice to perform elasticity measurements through oscillatory experiments, dynamic mechanical analysis (DMA), as well as the instrument used to carry out these experiments, the Perkin Elmer series 7 dynamic mechanical analyser. Porous glasses employed in our experimental work (Vycor 7930 and Gelsil) are also described in this chapter alongside salol (phenyl salicylate), the low molecular weight glass-forming liquid that we investigated. The sample preparation for our experiments is also presented in detail herein.

The third chapter of this thesis includes our published work on the heterogeneous relaxation dynamics of nanoconfined salol probed by DMA. Our low-frequency measurements of the elastic susceptibility of salol confined to Vycor glass demonstrate that the dynamic elastic response of salol allows the separation of surface-induced slowing-down of the molecular dynamics and confinement-induced acceleration effects.

The fourth chapter focuses on our published results describing confinement effects on glass forming liquids probed by DMA, including the negative pressure effects that are present, but quantitatively less important than the suppression of the cooperative motion, which is the main effect of confinement to porous Vycor and Gelsil.

Finally, the fifth chapter constitutes a review of an array of subsequent applications and extensions of this work, including the study of other glass-forming liquids, the use of other nanoporous materials in similar studies, the use of mesoporous Gelsil and Vycor matrices with silanated pore surfaces, as well as various models to analyze such experimental data, and alternative experimental techniques.

Our first series of measurements demonstrates that DMA constitutes a very sensitive method to test the dynamic behaviour of glass-forming liquids in confined systems. This technique allows one to investigate if there is an “intrinsic” confinement or size effect that is compensated by surface effects. The results of our studies on salol indicate that for decreasing pore radius, the second anomaly in the loss modulus becomes more pronounced, and as such it makes it easier to distinguish confinement and surface effects for pore sizes that approach the correlation length, i.e. the size of the “cooperatively rearranging regions” within the material.

Our second series of measurements used DMA to assess the glass transition of salol confined to porous matrices of Vycor and Gelsil with pore sizes between 2.6 and 7.5 nm. We showed that our dynamic complex elastic susceptibility data can be fitted well assuming two types of dynamic processes, a "bulk" relaxation in the core of the pores and a radially increasing "surface relaxation" of molecules in the vicinity of the pore surface. The core relaxation time decreases with decreasing pore radius, and the confinement-induced acceleration of dynamics causes a shift of T_g inversely proportional to the pore radius. We also used measurements of the sample height with filling (adsorption swelling) and thermal expansion to calculate the effect of "negative pressure" due to thermal mismatch between the porous host matrix and the glass-forming liquid. Such negative pressure could explain at least in part a shift of T_g in confined glass-forming liquids. We showed that in the case of salol this effect could only describe up to 30% of the observed downshift of T_g. Consequently, we believe that the main cause for the T_g shift is a confinement-induced hindering of cooperativity.

The size dependence of the downshift of T_g is assumed to increase with increasing fragility. Indeed, our experiments confirm this correlation, and we presume that the main effect of the confinement is to suppress cooperative motion. Consequently, negative pressure effects, while always present, do not have a major contribution to the T_g shift in confinement.

Chapter 7

7. LIST OF FIGURES AND TABLES

7.1. List of Figures

7.2. List of Tables

Chapter 8

8. REFERENCES

1. E. K. H. Salje, W. Schranz, Low amplitude, low frequency elastic measurements using Dynamic Mechanical Analyzer (DMA) spectroscopy. *Zeitschrift für Kristallographie* **226**, 1-17 (2011).
2. N. G. McCrum, B. E. Read, G. Williams, Anelastic and dielectric effects in polymeric solids. Wiley, London (1967).
3. M. Reinecker, V. Soprunyuk, M. Fally, A. Sanchez-Ferrer, W. Schranz, Two glass transitions of polyurea networks: effect of the segmental molecular weight. *Soft Matter* **10**, 5729-5738 (2014).
4. E. A. Turi, Thermal characterization of polymeric materials. Academic Press, Brooklyn, New York, Second ed., Vol. I (1997).
5. P. G. Debenedetti, F. H. Stillinger, Supercooled liquids and the glass transition. *Nature* **410**, 259-267 (2001).
6. C. A. Angell, K. L. Ngai, G. B. McKenna, P. F. McMillan, S. W. Martin, Relaxation in glassforming liquids and amorphous solids. *Applied Physics Reviews* **88**, 3113–3157 (2000).
7. E. Hempel, A. Hempel, A. Hensel, G. Schick, E. Donth, Characteristic length of dynamic glass transition near Tg for a wide assortment of glass-forming substances. *The Journal of Physical Chemistry B* **104**, 2460-2466 (2000).
8. J. E. K. Schawe, Principles for the interpretation of modulated temperature DSC measurements. Part 1. Glass transition. *Thermochimica Acta* **261**, 183-194 (1995).
9. M. J. O'Neill, E. S. Watson, Differential microcalorimeter. Perkin Elmer Corp., asignee. U.S. patent 3263484 (1966).
10. P. L. Privalov, K. A. Kafiani, D. R. Monaselidze, [Study of Heat Denaturation of DNA by Use of the Adiabatic Microcalorimeter]. *Doklady Akademii nauk SSSR* **156**, 951-953 (1964).

11. A. Hensel, C. Schick, Relation between freezing-in due to linear cooling and the dynamic glass transition temperature by temperature-modulated DSC. *Journal of Non-Crystalline Solids* **235-237**, 510-516 (1998).
12. A. Hensel, Kalorimetrische Untersuchungen zum Zusammenhang zwischen dynamischem Glasübergang und Einfriervorgang. University of Rostock, Rostock. Ph.D. Thesis (2000).
13. B. Wunderlich, The thermal properties of complex, nanophase-separated macromolecules as revealed by temperature-modulated calorimetry. *Thermochimica Acta* **403**, 1-13 (2003).
14. P. Gill, T. T. Moghadam, B. Ranjbar, Differential scanning calorimetry techniques: applications in biology and nanoscience. *Journal of Biomolecular Techniques* **21**, 167-193 (2010).
15. M. Reading, Modulated differential scanning calorimetry – a new way forward in materials characterization. *Trends in polymer science* **8**, 248 (1993).
16. M. Reading, D. Elliot, V. L. Hill, A new approach to the calorimetric investigation of physical and chemical transitions. *Journal of Thermal Analysis and Calorimetry* **40**, 949-955 (1993).
17. P. H. Gill, S. R. Sauerbrunn, M. Reading, Modulated differential scanning calorimetry. *Journal of Thermal Analysis and Calorimetry* **40**, 931-939 (1993).
18. G. Adam, J. H. Gibbs, On the temperature dependence of cooperative relaxation properties in glass-forming liquids. *The Journal of Chemical Physics* **43**, 139-146 (1965).
19. W. Schranz, M. R. Puica, J. Koppensteiner, H. Kabelka, A. V. Kityk, Heterogeneous relaxation dynamics of nano-confined salol probed by DMA. *Europhysics Letters* **79: 36003**, (2007).
20. E. W. Fischer, E. Donth, W. Steffen, Temperature dependence of characteristic length for glass transition. *Physical Review Letters* **68**, 2344-2346 (1992).
21. L. Berthier *et al.*, Direct experimental evidence of a growing length scale accompanying the glass transition. *Science* **310**, 1797-1800 (2005).

22. M. Arndt, R. Stannarius, H. Groothues, E. Hempel, F. Kremer, Length scale of cooperativity in the dynamic glass transition. *Physical Review Letters* **79**, 2077-2080 (1997).
23. P. Pissis *et al.*, Dielectric studies of glass transition in confined propylene glycol. *Journal of Physics: Condensed Matter* **10**, 6205 (1998).
24. E. Russel, N. Israeloff, L. Walther, H. Gomariz, Nanometer scale dielectric fluctuations at the glass transition. *Physical Review Letters* **81**, 1461-1464 (1998).
25. B. Schiener, R. Böhmer, A. Loidl, R. Chamberlin, Nonresonant spectral hole burning in the slow dielectric response of supercooled liquids. *Science* **274**, 752-754 (1996).
26. E. W. Fischer, Light scattering and dielectric studies on glass forming liquids. *Physica A* **201**, 183-206 (1993).
27. C. T. Moynihan, J. J. Schroeder, Non-exponential structural relaxation, anomalous light scattering and nanoscale inhomogeneities in glass-forming liquids. *Journal of Non-Crystalline Solids* **160**, 52-59 (1993).
28. X. H. Qiu, M. D. Edinger, Length scale of dynamic heterogeneity in supercooled D-sorbitol: Comparison to model predictions. *The Journal of Physical Chemistry B* **107**, 459-464 (2003).
29. S. A. Reinsberg, A. Heuer, B. Doliwa, H. Zimmermann, H. W. Spiess, Comparative study of the NMR length scale of dynamic heterogeneities of three different glass formers. *Journal of Non-Crystalline Solids* **307–310**, 208 (2002).
30. K. Schmidt-Rohr, H. W. Spiess, Nature of nonexponential loss of correlation above the glass transition investigated by multidimensional NMR. *Physical Review Letters* **66**, 3020-3023 (1991).
31. A. Heuer, M. Wilhelm, H. Zimmermann, H. W. Spiess, Rate memory of structural relaxation in glasses and its detection by multidimensional NMR. *Physical Review Letters* **75**, 2851-2854 (1995).
32. U. Tracht *et al.*, Length scale of dynamic heterogeneities at the glass transition determined by multidimensional nuclear magnetic resonance. *Physical Review Letters* **81**, 2727-2730 (1998).

33. A. Mel'cuk, R. Ramos, H. Gould, W. Klein, R. Mountain, Long-lived structures in fragile glass-forming liquids. *Physical Review Letters* **75**, 2522-2525 (1995).

34. J. Horbach, W. Kob, K. Binder, C. A. Angell, Finite size effects in simulations of glass dynamics. *Physical Review E* **54**, R5897-R5900 (1996).

35. P. K. Dixon, L. Wu, S. R. Nagel, B. D. Williams, J. P. Carini, Scaling in the relaxation of supercooled liquids. *Physical Review Letters* **65**, 1108-1111 (1990).

36. G. Li, W. M. Du, A. Sakai, H. Z. Cummins, Light-scattering investigation of α and β relaxation near the liquid-glass transition of the molecular glass Salol. *Physical Review A* **46**, 3343–3356 (1992).

37. G. Binnig, C. F. Quate, C. Gerber, Atomic Force Microscope. *Physical Review Letters* **56**, 930-933 (1986).

38. R. Böhmer *et al.*, Nature of the non-exponential primary relaxation in structural glass-formers probed by dynamically selective experiments. *Journal of Non-Crystalline Solids* **235-237**, 1-9 (1998).

39. H. Sillescu, Heterogeneity at the glass transition: a review. *Journal of Non-Crystalline Solids* **243**, 81-108 (1999).

40. K. Schmidt-Rohr, H. W. Spiess, Multidimensional solid-state NMR and polymers. Academic Press, London (1994).

41. S. A. Reinsberg, X. H. Qiu, M. Wilhelm, H. W. Spiess, M. D. Edinger, Length scale of dynamic heterogeneity in supercooled glycerol near Tg. *The Journal of Chemical Physics* **114**, 7299-7302 (2001).

42. C. A. Angell, Strong and fragile liquids. In Relaxations in complex systems, K. L. Ngai and G. B. Wright, Eds., Research Laboratory, Springfield (1985).

43. K. P. Menard, Dynamic mechanical analysis: A practical introduction. CRC Press, Boca Raton, Florida, Second ed. (2008).

44. R. W. Carpick, N. Agrait, D. F. Ogletree, e. al., Variation of the interfacial shear strength and adhesion of a nanometer-sized contact. *Langmuir* **12**, 3334–3340 (1996).

45. J. P. Salvetat *et al.*, Mechanical properties of carbon nanotubes. *Applied Physics A* **69**, 255-260 (1999).

46. Z. Cheng, T. G. Mason, P. M. Chaikin, Periodic oscillation of a colloidal disk near a wall in an optical trap. *Physical Review E - Statistical, Nonlinear, and Soft Matter Physics* **68**, 051404 (2003).

47. T. Mora, H. Yu, Y. Sowa, N. S. Wingreen, Steps in the bacterial flagellar motor. *PLOS Computational Biology* **5**, e1000540 (2009).

48. K. Svoboda, S. M. Block, Biological applications of optical forces. *Annual Review of Biophysics and Biomolecular Structure* **23**, 247-285 (1994).

49. K. Visscher, S. M. Block, Versatile optical traps with feedback control. *Methods in Enzymology* **298**, 460-489 (1998).

50. J. H. Poynting, On pressure perpendicular to the shear planes in finite pure shears, and on the lengthening of loaded wires when twisted. *Proceedings of the Royal Society of London, Series A* **82**, 546-559 (1909).

51. A. Kimball, D. Lovell, Internal friction in solids. *Transactions of the American Society of Mechanical Engineers* **48**, 479 (1926).

52. K. te Nijenhuis, Rheology, Volume 1: Principles. G. Astarita, Ed., Plenum Press, New York (1980).

53. J. D. Ferry, Viscoelastic properties of polymers. Wiley, New York (1961).

54. M. L. Miller, The structure of polymers. Reinhold, New York (1966).

55. J. Gillham, J. Enns, On the cure properties of thermosetting polymers using torsional braid analysis. *Trends in polymer science* **2**, 406-419 (1994).

56. L. E. Nielson, A recording torsion pendulum for the measurement of the dynamic mechanical properties of plastics and rubbers. *Review of Scientific Instruments* **22**, 690-693 (1951).

57. G. T. Gillies, R. C. Ritter, Torsion balances, torsion pendulums, and related devices. *Review of Scientific Instruments* **64**, 283-309 (1993).

58. I. Jackson, A. Barnhoorn, Y. Aizawa, e. al., Improved procedures for the laboratory study of high-temperature viscoelastic relaxation. *Physics of the Earth and Planetary Interiors* **172**, 104-115 (2009).

59. Q. L. Wang, H. C. Yeh, Z. B. Zhou, e. al., Improving the sensitivity of a torsion pendulum by using an optical spring method. *Physical Review A* **80: 043811**, (2009).

60. A. D. Mehta, M. Rief, J. A. Spudich, D. A. Smith, R. M. Simmons, Single-molecule biomechanics with optical methods. *Science* **283**, 1689-1695 (1999).

61. E. R. Dufresne , D. G. Grier, Optical tweezer arrays and optical substrates created with diffractive optics. *Review of Scientific Instruments* **69**, 1974–1977 (1998).

62. C. Ortiz, G. Hadziioannou, Entropic elasticity of single polymer chains of poly(methacrylic acid) measured by atomic force microscopy. *Macromolecules* **32**, 780–787 (1999).

63. D. Van Krevelen, Properties of polymers. Elsevier, New York (1972).

64. R. H. Boyd, Relaxation processes in crystalline polymers: experimental behavior. *Polymer* **26**, 323 (1985).

65. R. H. Boyd, Relaxation processes in crystalline polymers: molecular interpretation – a review. *Polymer* **26**, 1123 (1985).

66. N. G. McCrum, G. Williams, B. Read, Anelastic and dielectric effects in polymeric solids. Dover, New York (1991).

67. B. Twombly, K. Fielder, R. Cassel, W. Brennan, Dynamic mechanical analysis of elastomers. *North American Thermal Analysis Society Proceedings* **20**, 28 (1991).

68. B. Cassel, B. Twombly, Glass transition determination by thermomechanical analysis, a dynamic mechanical analyzer, and a differential scanning calorimeter. In ASTM, M. Neag, Ed., Philadelphia, STP1136, pp. 1108-1119 (1991).

69. T. M. Nair, M. G. Kumaran, G. Unnikrishnan, V. B. Pillai, Dynamic mechanical analysis of ethylene-propylene-diene monomer rubber and styrene-butadiene rubber blends. *Journal of Applied Polymer Science* **112**, 72-81 (2009).

70. S. Crane, B. Twombly, Optimization of epoxy cure using a dynamic cure scan. *North American Thermal Analysis Society Proceedings* **20**, 386 (1991).

71. K. M. Hollands, I. L. Kalnin, The kinetics of gelation of some accelerated acid anhydride cured epoxy resins. *Advances in Chemistry Series* **92**, 60-69 (1970).

72. M. B. Roller, Characterization of the time-temperature-viscosity behaviour of curing B-staged epoxy resin. *Polymer Engineering & Science* **15**, 406-414 (1975).

73. C. Rohm, *Proceedings of the 1988 Hot Melt Symposium*, p. 77 (1988).

74. R. R. Rahalkar, H. Tang, Prediction of zero-shear viscosity of linear polybutadienes from the crossover point using Doi-Edwards theory. *Rubber Chemistry and Technology* **61**, 812-827 (1988).

75. R. R. Rahalkar, Correlation between the crossover modulus and the molecular weight distribution using the Doi-Edwards theory of reptation and the Rouse theory. *Rheologica Acta* **28**, 166-175 (1989).

76. W. Tuminello, Molecular weight and molecular weight distribution from dynamic measurements of polymer melts. *Polymer Engineering & Science* **26**, 1339-1347 (1986).

77. L. Nielsen, Mechanical properties of polymers. Reinhold, New York (1965).

78. L. Nielsen, Mechanical properties of polymers and composites. Marcel Dekker, New York, vol. 1 (1974).

79. U. Zolzer, H. Eicke, Free oscillatory sheer measurements – an interesting application of constant stress rheometers in the creep mode. *Rheologica Acta* **32**, 104-107 (1993).

80. R. E. Wetton, R. D. L. Marsh, J. G. Van-de-Velde, Theory and application of dynamic mechanical thermal analysis. *Thermochimica Acta* **175**, 1-11 (1991).

81. J. Koppensteiner, The glass transition in nanoscaled confinement probed by dynamic mechanical spectroscopy. University of Vienna, Vienna, Ph.D. Thesis (2009).

82. A. V. Kityk *et al.*, Low frequency superelasticity and nonlinear elastic behaviour of SrTiO3 crystals. *Physical Review B* **61**, 946-956 (2000).

83. Measurement of the glass transition temperature using dynamic mechanical analysis. http://www.tainstruments.com/pdf/literature/TS64.pdf (Accessed August 21, 2016).

84. J. Koppensteiner, W. Schranz, M. R. Puica, Confinement effects on glass forming liquids probed by dynamic mechanical analysis. *Physical Review B* **78: 054203**, (2008).

85. T. H. Elmer, Porous and reconstructed glasses. In "Engineered Materials Handbook", Vol. 4: Ceramics and Glasses, pp. 427-432 (1992).

86. W. E. S. Turner, F. Winks, The influence of boric oxide on the properties of chemical and heat-resisting glasses. *Journal of the Society of Glass Technology* **10**, 102-113 (1926).

87. H. P. Hood, M. E. Nordberg, Treated borosilicate glass. Corning Glass Works, asignee. U.S. patent 2106744 (1938).

88. T. H. Elmer, Porous and reconstructed glasses. In Engineered Materials Handbook, Vol. 4, Ceramic and Glasses, ASM International, Materials Park, OH, 427-432 (1992).

89. P. Levitz, G. Ehret, S. K. Sinha, J. M. Drake, Porous vycor glass: The microstructure as probed by electron microscopy, direct energy transfer, small ‐ angle scattering, and molecular adsorption. *The Journal of Chemical Physics* **95**, 6151-6161 (1991).

90. F. Somorowsky, B. Durschang, M. Kilo, G. Sextl, Porous Vycor glass: Interrelation between morphology, structure and water uptake. http://www2.thphy.uni-duesseldorf.de/briscagla1/files/ferdinand_somorowsky.pdf (Accessed July 10, 2016).

91. S. Brunauer, P. H. Emmett, E. Teller, Adsorption of Gases in Multimolecular Layers. *The Journal of the American Chemical Society* **60**, 309-319 (1938).

92. A. Feinle, M. S. Elsaesser, N. Hüsing, Sol–gel synthesis of monolithic materials with hierarchical porosity. *Chemical Society Reviews* **45**, 3377-3399 (2016).

93. L. B. McCusker, F. Liebau, G. Engelhardt, Nomenclature of structural and compositional characteristics of ordered microporous and mesoporous materials with inorganic hosts (IUPAC Recommendations 2001). *Pure and Applied Chemistry* **73**, 381-394 (2001).

94. A. Alvarez-Herrero, R. L. Heredero, E. Bernabeu, D. Levy, Adsorption of water on porous Vycor glass studied by ellipsometry. *Applied Optics* **40**, 527-532 (2001).

95. K. L. Stefanopoulos, A. C. Mitropoulos, E. S. Kikkinides, N. K. Kanellopoulos, A. Christoforides, Study of themacroporosity of Vycor porous glass by combining scattering and permeability techniques. *Applied Physics A* **74**, S1336-S1338 (2002).

96. J. Koppensteiner, W. Schranz, M. A. Carpenter, Revealing the pure confinement effect in glass-forming liquids by dynamic mechanical analysis. *Physical Review B* **81: 024202**, (2010).

97. C. Streck, Y. B. Mel'nicenko, R. Richert, Dynamics of solvation in supercooled liquids confined to the pores of sol-gel glasses. *Physical Review B* **53**, 5341-5347 (1996).

98. H. Wendt, R. Richert, Cooperativity and heterogeneity of the dynamics in nano-confined liquids *Journal of Physics: Condensed Matter* **11**, A199-A206 (1999).

99. N. Eschricht, E. Hoinkis, F. Mädler, P. Schubert-Bischoff, B. Röhl-Kuhn, Knowledge-based reconstruction of random porous media. *Journal of Colloid and Interface Science* **291**, 201-213 (2005).

100. J. L. R. Nogues, W. V. Moreshead, Porous gel-silica, a matrix for optically-active components. *Journal of Non-Crystalline Solids* **121**, 136-142 (1990).

101. Deutsche Normen, Bestimmung der dichtekörniger und pulverförmiger Stoffe mit dem Pyknometer. Beuth Vertrieb GmbH, Berlin (1969).

102. W. Zheng, S. L. Simon, Confinement effects on the glass transition of hydrogen bonded liquids. *The Journal of Chemical Physics* **127**, 194501 (2007).

103. N. Eschricht, E. Hoinkis, F. Mädler, Nitrogen distribution at 77.7 K in mesoporous Gelsil 50 generated via evolutionary minimization with statistical descriptors derived from adsorption and in situ SANS. *Langmuir* **23**, 2145-2157 (2007).

104. R. Zorn, L. Hartmann, B. Frick, D. Richter, F. Kremer, Inelastic neutron scattering experiments on the dynamics of a glass-forming material in

mesoscopic confinement. *Journal of Non-Crystalline Solids* **307-310**, 547-554 (2002).

105. K. Adrjanowicz *et al.*, Decoupling between the interfacial and core molecular dynamics of salol in 2D confinement. *Journal of Physical Chemistry C* **119**, 14366-14374 (2015).
106. P. H. Laswick, Freezing curves for Salol. *Journal of Chemical Education* **49**, (1972).
107. D. H. Torchinsky, J. A. Johnson, K. A. Nelson, A direct test of the correlation between elastic parameters and fragility of ten glass formers and their relationship to elastic models of the glass transition. *The Journal of Chemical Physics* **130**, 064502 (2009).
108. C. A. Angell, Formation of glasses from liquids and biopolymers. *Science* **267**, 1924-1935 (1995).
109. M. D. Marvin, R. J. Lang, D. S. Simmons, Nanoconfinement effects on the fragility of glass formation of a model freestanding polymer film. *Soft Matter* **10**, 3166-3170 (2014).
110. V. N. Novikov, A. P. Sokolov, Poisson's ratio and fragility of glass-forming liquids. *Nature* **431**, 961-963 (2004).
111. V. N. Novikov, Y. Ding, A. P. Sokolov, Correlation of fragility of supercooled liquids with elastic properties of glasses. *Physical Review E* **71**, 061501 (2005).
112. T. Scopigno, G. Ruocco, F. Sette, G. Monaco, Is the fragility of a liquid embedded in the properties of its glass? *Science* **302**, 849-852 (2003).
113. R. Böhmer, K. L. Ngai, C. A. Angell, D. J. Plazek, Nonexponential relaxations in strong and fragile glass formers. *The Journal of Chemical Physics* **99**, 4201 (1993).
114. C. M. Evans, Fragility is a key parameter in determining the magnitude of Tg-confinement effects in polymer films. *Macromolecules* **46**, 6091-6103 (2013).
115. P. Z. Hanakata, J. F. Douglas, F. W. Starr, Local variation of fragility and glass transition temperature of ultra-thin supported polymer films. *Journal of Chemical Physics* **137**, 244901 (2012).

116. R. A. Riggleman, K. Yoshimoto, J. F. Douglas, J. J. de Pablo, Influence of confinement on the fragility of antiplasticized and pure polymer films. *Physical Review Letters* **97**, 045502 (2006).

117. C. Zhang, Y. Guo, K. B. Shepard, R. D. Priestley, Fragility of an Isochorically Confined Polymer Glass. *The Journal of Physical Chemistry Letters* **4**, 431-436 (2013).

118. C. Zhang, R. D. Priestley, Fragility and glass transition temperature of polymer confined under isobaric and isochoric conditions. *Soft Matter* **9**, 7076-7085 (2013).

119. Y. P. Koh, S. L. Simon, Structural relaxation of stacked utrathin polystyrene films. *Journal of Polymer Science: Part B: Polymer Physics* **46**, 2741 - 2753 (2008).

120. K. Fukao, Y. Miyamoto, Slow dynamics near glass transitions in thin polymer films. *Physical Review E* **64**, 011803 (2001).

121. S. Napolitano, M. Wübbenhorst, Structural relaxation and dynamic fragility of freely standing polymer films. *Polymer* **51**, 5309-5312 (2010).

122. G. S. Iannacchione, G. P. Crawford, S. Qian, J. W. Doane, D. Finotello, Nematic ordering in highly restrictive Vycor glass. *Physical Review E* **53**, 2402 (1996).

123. D. Wallacher, T. Hofmann, K. Knorr, A. V. Kityk, Dielectric response of HBr condensed into mesoporous glass. *Physical Review B* **71**, 224202 (2005).

124. C. L. Jackson, G. B. McKenna, Vitrification and crystallization of organic liquids confined to nanoscale pores. *Chemistry of Materials* **8**, 2128-2137 (1996).

125. V. P. Soprunyuk, D. Wallacher, P. Huber, K. Knorr, A. V. Kityk, Freezing and melting of Ar in mesopores studied by optical transmission. *Physical Review B* **67**, 144105 (2003).

126. D. Wallacher, V. Soprunyuk, K. Knorr, A. V. Kityk, Dielectric response of acetonitrile condensed into mesoporous. *Physical Review B* **69**, 134207 (2004).

127. D. Wallacher, K. Knorr, Melting and freezing of Ar in nanopores. *Physical Review B* **63**, 104202 (2001).

128. B. Frick, M. Koza, R. Zorn, Dynamics in Confinement. *The European Physical Journal E* **12**, 3-4 (2003).

129. M. Cukierman, J. W. Lane, D. R. Uhlmann, High‐temperature flow behavior of glass‐forming liquids: A free‐volume interpretation. *Journal of Chemical Physics* **59**, 3639 (1973).

130. M. D. Ediger, C. A. Angell, S. R. Nagel, Supercooled liquids and glasses. *Journal of Physical Chemistry* **100**, 13200-13212 (1996).

131. J. Jäckle, A. Krönig, A kinetic lattice-gas model for the triangular lattice with strong dynamic correlations. I. Self-diffusion. *Journal of Physics: Condensed Matter* **6**, 7633 (1994).

132. R. Richert, Geometrical confinement and cooperativity in supercooled liquids studied by solvation dynamics. *Physical Review B* **54**, 15762 (1996).

133. B. Frick, R. Zorn, H. Büttner, (editors), In Proceedings of the International Workshop on Dynamics in Confinement. *Le Journal de Physique IV* **10**, 3-346 (2000).

134. A. Schönhals, H. Goering, C. H. Schick, B. Frick, R. Zorn, Glassy dynamics of polymers confined to nanoporous glasses revealed by relaxational and scattering experiments. *The European Physical Journal E* **12**, 173-178 (2003).

135. C. L. Jackson, G. B. McKenna, The glass transition of organic liquids confined to small pores. *Journal of Non-Crystalline Solids* **131-133**, 221-224 (1991).

136. O. Trofymluk, A. A. Levchenko, A. Navrotsky, Interfacial effects on vitrification of confined glass-forming liquids. *Journal of Chemical Physics* **123: 194509**, (2005).

137. E. Donth, E. Hempel, C. Schick, Does temperature fluctuate? Indirect proof by dynamic glass transition in confined geometries. *Journal of Physics: Condensed Matter* **12**, L281–L286 (2000).

138. B. Frick *et al.*, Inelastic neutron scattering for investigating the dynamics of confined glass forming liquids. *Journal of Non-Crystalline Solids* **351**, 2657-2667 (2005).

139. C. Alba-Simionesco *et al.*, Confinement of molecular liquids: Consequences on thermodynamic, static and dynamical properties of benzene and toluene. *The European Physical Journal E* **12**, 19-28 (2003).

140. M. Alcoutlabi, G. B. McKenna, Effects of confinement on material behaviour at the nanometre size scale. *Journal of Physics: Condensed Matter* **17**, R461-R524 (2005).

141. P. Scheidler, W. Kob, K. Binder, The relaxation dynamics of a simple glass former confined in a pore. *Europhysics Letters* **52**, 277-283 (2002).

142. P. Scheidler, W. Kob, K. Binder, Cooperative motion and growing length scales in supercooled confined liquids. *Europhysics Letters* **59**, 701-707 (2002).

143. P. Scheidler, W. Kob, K. Binder, G. Parisi, Growing length scales in a supercooled liquid close to an interface. *Philosophical Magazine B* **82**, 283-290 (2002).

144. P. Scheidler, W. Kob, K. Binder, The relaxation dynamics of a confined glassy simple liquid. *The European Physical Journal E* **12**, 5-9 (2003).

145. H. Huth, M. Beiner, E. Donth, Temperature dependence of glass-transition cooperativity from heat-capacity spectroscopy: Two post-Adam-Gibbs variants. *Physical Review B* **61**, 15092 (2000).

146. A. Faivre, L. David, J. Perez, Study of the α-mechanical relaxation in molecular glass-forming liquids. *Journal de Physique II* **7**, 1635-1650 (1997).

147. F. Kremer, A. Huwe, A. Schönhals, A. S. Rzanski, Molecular dynamics in confining space. In Broadband Dielectric Spectroscopy, F. Kremer and A. Schönhals, eds., Springer-Verlag, Berlin, p. 171 (2000).

148. J. C. Dore, M. Dunn, T. Hasebe, J. H. Strange, M. C. Belissent-Funel, Dynamics of disordered materials. D. Richter, ed., Springer-Verlag, Berlin (1989).

149. G. Liu, Y. Li, J. Jonas, Confined geometry effects on reorientational dynamics of molecular liquids in porous silica glasses. *The Journal of Chemical Physics* **95**, 6892-6901 (1991).

150. Y.-J. Park, G. B. McKenna, Size and confinement effects on the glass transition behavior of polystyrene/o-terphenyl polymer solutions. *Physical Review B* **61**, 6667-6676 (2000).
151. C. Alba-Simionesco *et al.*, Effects of confinement on freezing and melting. *Journal of Physics: Condensed Matter* **18**, R15-68 (2006).
152. H. Wagner, R. Richert, Dielectric beta relaxations in the glassy state of salol? *The Journal of Chemical Physics* **110**, 11660 (1999).
153. W. Schranz, Dynamic mechanical analysis—a powerful tool for the study of phase transitions. *Phase Transitions* **64**, 103-114 (1997).
154. W. Schranz, D. Havlik, Heat-diffusion central peak in the elastic susceptibility of KSCN. *Physical Review Letters* **73**, 2575 (1994).
155. K. Niss, B. Jakobsen, N. B. Olsen, Dielectric and shear mechanical relaxations in glass-forming liquids: a test of the Gemant-DiMarzio-Bishop model. *The Journal of Chemical Physics* **123**, 234510 (2005).
156. P. A. O'Connell, G. B. McKenna, Arrhenius-type temperature dependence of the segmental relaxation below Tg. *The Journal of Chemical Physics* **110**, 11054 (1999).
157. M. Tabellout *et al.*, Glass-transition dynamics of a polyurethane gel using ultrasonic spectroscopy, dynamic light scattering, and dynamical mechanical thermal analysis. *Physical Review B* **51**, 12295 (1995).
158. O. Ishai, L. J. Cohen, Elastic properties of filled and porous epoxy composites. *International Journal of Mechanical Sciences* **9**, 539-546 (1967).
159. E. M. Schulson, The structure and mechanical behavior of ice. *JOM* **51**, 21-27 (1999).
160. E. J. Sellevold, F. Radjy, Low temperature dynamic mechanical response of porous Vycor glass as a function of moisture content. *Journal of Materials Science* **11**, 1927-1938 (1976).
161. M. Arndt, R. Stannarius, W. Gorbatschow, F. Kremer, Dielectric investigations of the dynamic glass transition in nanopores. *Physical Review E* **54**, 5377–5390 (1996).

162. P. K. Dixon, Specific-heat spectroscopy and dielectric susceptibility measurements of salol at the glass transition. *Physical Review B* **42**, 8179 (1990).

163. W. Kauzmann, The nature of the glassy state and the behavior of liquids at low temperatures. *Chemical Reviews* **43**, 219-256 (1948).

164. C. Donati *et al.*, Stringlike cooperative motion in a supercooled liquid. *Physical Review Letters* **80**, 2338 (1998).

165. C. Bennemann, C. Donati, J. Baschnagel, S. C. Glotzer, Growing range of correlated motion in a polymer melt on cooling towards the glass transition. *Nature* **399**, 246-249 (1999).

166. G. Biroli, J. P. Bouchaud, K. Miyazaki, D. R. Reichman, Inhomogeneous mode-coupling theory and growing dynamic length in supercooled liquids. *Physical Review Letters* **97**, 195701 (2006).

167. E. Donth, H. Huth, M. Beiner, Characteristic length of the glass transition. *Journal of Physics: Condensed Matter* **13**, L451 (2001).

168. R. Bergman, J. Swenson, Dynamics of supercooled water in confined geometry. *Nature* **403**, 283-286 (2000).

169. J. C. Dore, M. Dunn, T. Hasebe, J. H. Strange, M. C. Belissent-Funel, Structure and dynamics of cyclohexane in bulk and constrained geometry. In Dynamics of Disordered Materials, D. Richter, A.J. Dianoux, W. Petry and J. Teixeira eds., Springer-Verlag, 37, 144 (1989).

170. P. Huber, K. Knorr, Solidified fillings of nanopores. *Materials Research Society Symposium Proceedings* **876E**, R3.1 (2005).

171. A. V. Kityk, T. Hofmann, K. Knorr, Liquid-vapor coexistence at a mesoporous substrate. *Physical Review Letters* **100**, 036105 (2008).

172. A. Schönhals, H. Goering, C. Schick, B. Frick, R. Zorn, Glass transition of polymers confined to nanoporous glasses. *Colloid and Polymer Science* **282**, 882-891 (2004).

173. F. Kremer, A. Huwe, A. Schönhals, Molecular Dynamics in Confining Space. In Broadband Dielectric Spectroscopy, F. Kremer and A. Schönhals, eds., Springer-Verlag, Berlin, Heidelberg, 171-224 (2003).

174. A. Patkowski, T. Ruths, E. W. Fischer, Dynamics of supercooled liquids confined to the pores of sol-gel glass: A dynamic light scattering study.

Physical Review E - Statistical, Nonlinear, and Soft Matter Physics **67: 021501**, (2003).

175. E. Donth, The glass transition. Springer Verlag, Heidelberg (2001).

176. K. Kim, R. Yamamoto, Apparent finite-size effects in the dynamics of supercooled liquids. *Physical Review E* **61**, R41 (2000).

177. S. Karmakar, C. Dasgupta, S. Sastry, Growing length and time scales in glass forming liquids. *Proceedings of the National Academy of Sciences of the United States of America* **106**, 3675-3679 (2000).

178. F. Rouquerol, J. Rouquerol, K. Sing, Adosorption by powders and porous solids: Priciples, methodology and applications. Academic Press, New York (1999).

179. K. P. Menard, Encyclopedia of chemical processing. Taylor and Francis, London, 799 (2006).

180. W. Gorbatschow, M. Arndt, R. Stannarius, F. Kremer, Dynamics of H-bonded liquids confined to nanopores. *Europhysics Letters* **35**, 719 (1996).

181. D. Sappelt, J. Jäckle, The cooperativity length in models for the glass transition. *Journal of Physics A: Mathematical and General* **26**, 7325 (1993).

182. F. Kremer, R. Stannarius, Molecular dynamics of liquids in confinement. *Lecture Notes in Physics* **634**, 275-300 (2004).

183. A. G. Kalampounias, S. N. Yannopoulos, W. Steffen, L. I. Kirillova, Short-time dynamics of glass-forming liquids: Phenyl salicylate (salol) in bulk liquid, dilute solution, and confining geometries. *The Journal of Chemical Physics* **118**, 8340-8349 (2003).

184. E. Eckstein *et al.*, X-ray scattering study and molecular simulation of glass forming liquids: Propylene carbonate and salol. *The Journal of Chemical Physics* **113**, 4751-4762 (2000).

185. G. Diezemann, K. Nelson, Nonexponential primary relaxation in supercooled salol. *The Journal of Physical Chemistry B* **103**, 4089-4096 (1999).

186. R. Lucas, Ueber das Zeitgesetz des Kapillaren Aufstiegs von Flussigkeiten. *Kolloid-Zeitschrift* **23**, 15-22 (1918).

187. E. W. Washburn, The dynamics of capillary flow. *Physical Review* **17**, 273 (1921).

188. P. Huber, S. Grüner, C. Schäfer, K. Knorr, A. V. Kityk, Rheology of liquids in nanopores: A study on the capillary rise of water, n-Hexadecane and n-Tetracosane in mesoporous silica. *The European Physical Journal-Special Topics* **141**, 101-105 (2007).

189. D. I. Dimitrov, A. Milchev, K. Binder, Capillary rise in nanopores: Molecular dynamics evidence for the Lucas-Washburn equation. *Physical Review Letters* **99**, 054501 (2007).

190. F. T. Meehan, The expansion of charcoal on sorption of carbon dioxide. *Proceedings of the Royal Society of London. Series A, Containing Papers of a Mathematical and Physical Character* **115**, 199-207 (1927).

191. L. D. Landau, E. M. Lifschitz, Lehrbuch der Theoretischen Physik VI, Hydrodynamik. Akademie-Verlag, Berlin (1966).

192. D. P. Bentz, E. J. Garboczi, D. A. Quenard, Modelling drying shrinkage in reconstructed porous materials: application to porous Vycor glass. *Modelling and Simulation in Materials Science and Engineering* **6**, 211-236 (1998).

193. J. Zhang, G. Liu, J. Jonas, Effects of confinement on the glass transition temperature of molecular liquids. *The Journal of Physical Chemistry* **96**, 3478–3480 (1992).

194. C. L. Jackson, G. B. McKenna, The melting behavior of organic materials confined in porous solids. *The Journal of Chemical Physics* **93**, 9002-9011 (1990).

195. S. L. Simon, J.-Y. Park, G. B. McKenna, Enthalpy recovery of a glass-forming liquid constrained in a nanoporous matrix: Negative pressure effects. *The European Physical Journal E* **8**, 209-216 (2002).

196. H. Kamioka, Elastic behaviour of salol during melting and solidification processes. *Japanese Journal of Applied Physics* **32 Part 1**, 2216-2219 (1993).

197. R. Casalini, M. Paluch, C. M. Roland, Dynamics of salol at elevated pressure. *The Journal of Physical Chemistry A* **107**, 2369-2373 (2003).

198. D. Morineau, X. Yongde, C. Alba-Simionesco, Finite-size and surface effects on the glass transition of liquid toluene confined in cylindrical mesopores. *Journal of Chemical Physics* **117**, 8966 (2002).

199. A. Hunt, Finite-size effects on the glass transition temperature. *Solid State Communications* **90**, 527-532 (1994).

200. R. Richert, C. A. Angell, Dynamics of glass-forming liquids. V. On the link between molecular dynamics and configurational entropy. *The Journal of Chemical Physics* **108**, 9016 (1998).

201. J. Koppensteiner, W. Schranz, Dynamic mechanical analysis of confined glass-forming liquids. *Phase Transitions* **83**, 744-757 (2010).

202. A. V. Kityk, P. Huber, R. Pelster, K. Knorr, Spatial variation of molecular dynamics in the nanoconfined glass-former methanol. *The Journal of Physical Chemistry C* **118**, 12548-12554 (2014).

203. T. Blochowicz, E. Gouirand, S. Schramm, B. Stühn, Density and confinement effects of glass forming m-toluidine in nanoporous Vycor investigated by depolarized dynamic light scattering. *The Journal of Chemical Physics* **138: 114501**, (2013).

204. J. Schuller, Y. B. Mel'nichenko, R. Richert, E. W. Fischer, Dielectric studies of the glass transition in porous media. *Physical Review Letters* **73**, 2224–2227 (1994).

205. Y. B. Mel'nichenko, J. Schuller, R. Richert, B. Ewen, C. Loong, Dynamics of hydrogen-bonded liquids confined to mesopores: a dielectric and neutron spectroscopy study. *Journal of Chemical Physics* **103**, 2016–2024 (1995).

206. G. B. McKenna, Confit III: Summary and perspectives on dynamics in confinement. *The European Physical Journal Special Topics* **141**, 291-300 (2007).

207. J. K. Krüger, R. Holtwick, A. le Coutre, J. Baller, On the influence of nano-scaling on the glass transition of molecular liquids. *Nanostructured Materials* **12**, 519-522 (1999).

208. K. Binder, W. Kob, Glassy materials and disordered solids. World Scientific Publishing, Singapore (2011).

209. A. Kusmin *et al.*, Evidence of a sticky boundary layer in nanochannels: A neutron spin echo study of n-hexatriacontane and poly(ethylene oxide)

confined in porous silicon. *The Journal of Physical Chemistry Letters* **1**, 3116-3121 (2010).

210. R. Zorn, L. van Eijck, M. M. Koza, B. Frick, Progress in dynamics in confinement. *The European Physical Journal Special Topics* **189**, 1-2 (2010).

211. T. Hofmann *et al.*, Molecular dynamics of n-hexane: A quasi-elastic neutron scattering study on the bulk and spatially nanochannel-confined liquid. *The Journal of Chemical Physics* **136: 124505**, (2012).

212. A. Djemour, R. Sanctuary, J. Baller, Mobility restrictions and glass transition behaviour of an epoxy resin under confinement. *Soft Matter* **11**, 2683-2690 (2015).

213. G. Biroli, J. P. Bouchaud, A. Cavagna, T. S. Grigera, Thermodynamic signature of growing amorphous order in glass-forming liquids. *Nature Physics* **4**, 771-775 (2008).

214. P. Pissis, A. Kyritsis, G. Barut, R. Pelster, G. Nimtz, Glass transition in 2- and 3-dimensionally confined liquids. *Journal of Non-Crystalline Solids* **235-237**, 444-449 (1998).

215. T. R. Prisk, M. Tyagi, P. E. Sokol, Dynamics of small-molecule glass formers confined in nanopores. *The Journal of Chemical Physics* **134: 114506**, (2011).

216. G. Tsagaropoulos, A. Eisenburg, Direct observation of two glass transitions in silica-filled polymers. Implications to the morphology of random ionomers. *Macromolecules* **28**, 396-398 (1995).

217. A. Schönhals, F. Rittig, J. Kaerger, Self-diffusion of poly(propylene glycol) in nanoporous glasses studied by pulsed field gradient NMR: A study of molecular dynamics and surface interactions. *Journal of Chemical Physics* **133**, 094903 (2010).

218. B. J. Loughnane, R. A. Farrer, A. Scodinu, T. Reilly, J. T. Fourkas, Ultrafast spectroscopic studies of the dynamics of liquids confined in nanoporous glasses. *Journal of Physical Chemistry B* **104**, 5421-5429 (2000).

219. J. Baumert, B. Asmussen, C. Gutt, R. Kahn, Pore-size dependence of the self-diffusion of hexane in silica gels. *Journal of Chemical Physics* **116**, 10869-10876 (2002).

220. D. Wallacher, V. Soprunyuk, A. V. Kityk, K. Knorr, Dielectric response of Co and Ar condensed into mesoporous glass. *Physical Review B* **66**, 014203 (2002).

221. D. Morineau, R. Guegan, Y. D. Xia, C. Alba-Simionesco, Structure of liquid and glassy methanol confined in cylindrical pores. *Journal of Chemical Physics* **121**, 1466-1473 (2004).

222. P. Huber, Soft matter in hard confinement: phase transition thermodynamics, structure, texture, diffusion and flow in nanoporous media. *Journal of Physics: Condensed Matter* **27: 103102**, (2015).

223. R. R. Valiullin, V. D. Skirda, S. Stapf, R. Kimmich, Molecular exchange processes in partially filled porous glass as seen with NMR diffusometry. *Physical Review E* **55**, 2664-2671 (1997).

224. Q. Ji, R. Lefort, R. Busselez, D. Morineau, Structure and dynamics of a GayBerne liquid crystal confined in cylindrical nanopores. *Journal of Chemical Physics* **130: 234501**, (2009).

225. C. D. Norton, W. H. Thompson, Reorientation dynamics of nanoconfined acetonitrile: A critical examination of two-state models. *Journal of Physical Chemistry B* **118**, 8227-8235 (2014).

226. L. Li *et al.*, Glass transitions of poly(methyl methacrylate) confined in nanopores: conversion of three- and two-layer models. *The Journal of Physical Chemistry B* **119**, 5047−5054 (2015).

227. L. T. Canham, Silicon quantum wire array fabrication by electrochemical and chemical dissolution of wafers. *Applied Physics Letters* **57**, 1046-1048 (1990).

228. L. Canham, Ed., Handbook of porous silicon. Springer (2015).

229. V. Lehmann, U. Gsele, Porous silicon formation: A quantum wire effect. *Applied Physics Letters* **58**, 856 (1991).

230. A. G. Cullis, L. T. Canham, Visible-light emission due to quantum size effects in highly porous crystalline silicon. *Nature* **353**, 335-338 (1991).

231. C. T. Black *et al.*, Integration of self-assembled diblock copolymers for semiconductor capacitor fabrication. *Applied Physics Letters* **79**, 409-411 (2001).

232. M. J. Sailor, Porous silicon in practice - Preparation, characterization and applications. Wiley-VCH, Weinheim (2011).

233. F. Keller, M. S. Hunter, D. L. Robinson, Structural features of oxide coatings on aluminium. *Journal of the Electrochemical Society* **100**, 411-419 (1953).

234. H. Masuda, K. Fukuda, Ordered metal nanohole arrays made by a 2-step replication of honeycomb structures of anodic alumina. *Science* **268**, 1466-1468 (1995).

235. W. Lee, R. Ji, U. Gsele, K. Nielsch, Fast fabrication of long-range ordered porous alumina membranes by hard anodization. *Nature Materials* **5**, 741 (2006).

236. J. K. Holt *et al.*, Fast mass transport through sub-2-nanometer carbon nanotubes. *Science* **312**, 1034 (2006).

237. V. Presser, M. Heon, Y. Gogotsi, Carbide-derived carbons - from porous networks to nanotubes and graphene. *Advanced Functional Materials* **21**, (2011).

238. J. Erlebacher, M. J. Aziz, A. Karma, N. Dimitrov, K. Sieradzki, Evolution of nanoporosity in dealloying. *Nature* **410**, 450-453 (2001).

239. Z. Qi, J. Weissmueller, Hierarchical nested-network nanostructure by dealloying. *ACS Nano* **7**, 5948-5954 (2013).

240. P. C. A. Alberius *et al.*, General predictive syntheses of cubic, hexagonal, and lamellar silica and titania mesostructured thin films. *Chemistry of Materials* **14**, 3284-3294 (2002).

241. J. M. Macak, H. Tsuchiya, L. Taveira, S. Aldabergerova, P. Schmuki, Smooth anodic TiO2 nanotubes. *Angewandte Chemie-International Edition* **44**, 7463-7465 (2005).

242. K. Kolodziejczyk *et al.*, Crystallization kinetics under confinement. Manipulation of the crystalline form of salol by varying pore diameter. *Crystal Growth & Design* **16**, 1218-1227 (2016).

243. H. W. Spiess, Interplay of structure and dynamics in macromolecular and supramolecular systems. *Macromolecules* **43**, 5479–5491 (2010).

244. G. Dosseh, Y. Xia, C. Alba-Simionesco, Cyclohexane and benzene confined in MCM-41 and SBA-15: confinement effects on freezing and melting. *Journal of Physical Chemistry B* **107**, 6445-6453 (2003).

245. J. J. Moura Ramos, N. T. Correia, H. P. Diogo, Vitrification, nucleation and crystallization in phenyl-2-hidroxybenzoate (salol) studied by Differential Scanning Calorimetry (DSC) and Thermally Stimulated Depolarisation Currents (TSDC). *Physical Chemistry Chemical Physics* **6**, 793–798 (2004).
246. K. Adrjanowicz, K. Kaminski, K. Koperwas, M. Paluch, Pressure vitrification of the isochorically confined liquid in nanopores. *Physical Review Letters* **115: 265702**, (2015).

ACKNOWLEDGEMENTS

I would like to thank my supervisor, Prof. Dr. Wilfried Schranz, for giving me the opportunity to work in his *Physik Funktioneller Materialien* group, for introducing me to the exciting field of elastic properties of materials, and for his guidance and support throughout the experimental work and the writing of this thesis. I am also grateful to him for the post-doctoral researcher position he offered me in his group between 2006 and 2009, with financial support from his project Austrian FWF *Dynamische Elastizität komplexer Materialien* (P19284-N20).

I would also like to thank Prof. Dr. Andriy Kityk for initiating me in the use of DMA, for fruitful discussions, and for kindly sharing his knowledge and expertise in designing DMA experiments throughout the years.

I am thankful for the joy and balance my dear children Maria and Sebastian have brought me and for their understanding, support and encouragement during my studies at the Faculty of Mathematics over the last three years. It has been quite interesting to be a graduate student for the third time in my life, while at the same time my daughter (21 years old) is a student in International Business Administration, as well as Business Law, at the University of Economics and Business in Vienna, and my son (13 years old) is a middle school student.